10-29-2020

Recent advances in graphene-based materials for fuel cell applications

Hanrui Su
Michigan Technological University

Yun Hang Hu
Michigan Technological University, yunhangh@mtu.edu

Received: 20 August 2020 | Revised: 2 October 2020 | Accepted: 8 October 2020

DOI: 10.1002/ese3.833

REVIEW

Energy Science & Engineering
Open Access

Recent advances in graphene-based materials for fuel cell applications

Hanrui Su | **Yun Hang Hu**

Department of Materials Science and Engineering, Michigan Technological University, Houghton, MI, USA

Correspondence
Yun Hang Hu, Department of Materials Science and Engineering, Michigan Technological University, 1400 Townsend Drive, Houghton, MI 49931-1295, USA.
Email: yunhangh@mtu.edu

Funding information
NSF, Grant/Award Number: CMMI-1661699

Abstract

The unique chemical and physical properties of graphene and its derivatives (graphene oxide, heteroatom-doped graphene, and functionalized graphene) have stimulated tremendous efforts and made significant progress in fuel cell applications. This review focuses on the latest advances in the use of graphene-based materials in electrodes, electrolytes, and bipolar plates for fuel cells. The understanding of structure-activity relationships of metal-free heteroatom-doped graphene and graphene-supported catalysts was highlighted. The performances and advantages of graphene-based materials in membranes and bipolar plates were summarized. We also outlined the challenges and perspectives in using graphene-based materials for fuel cell applications.

KEYWORDS

bipolar plates, electrocatalyst, fuel cell, graphene, oxygen reduction reaction, polymer membrane

1 | INTRODUCTION

Fuel cells are a series of energy conversion devices that produce electricity as long as fuels are supplied. Since the chemical energy of fuels is directly converted to electricity, the system efficiency of fuel cells is significantly higher than the combustion engine, along with the low emission of pollutants. Therefore, fuel cells are considered as one of the attractive technologies to address global energy and environmental issues and make our lives cleaner and more sustainable. A typical fuel cell contains an electrolyte layer being sandwiched by two electrodes (Figure 1).[1] The fuel is oxidized on the anode surface, and the released electrons flow via an external circuit to reduce O_2 at the cathode. The mobile charge carriers (H^+, OH^-, CO_3^{2-}, or O^{2-}) simultaneously transfer through electrolytes to complete the circuit. According to the types of electrolytes, the fuels are classified as phosphoric acid fuel cell (PAFC), polymer electrolyte membrane fuel cell (PEMFC), alkaline fuel cell (AFC), molten carbonate fuel cell (MCFC), and solid-oxide fuel cell (SOFC).[1] Among these, PAFC, PEMFC, and AFC normally operate at relatively low temperatures (<300°C) and suitable for vehicles and portable applications, while MCFC and SOFC can utilize various fuels due to high operating temperatures (≥ 500°C) and be promising for stationary applications.

The material selection for fuel cell components faces the challenges in electrochemical performance, efficiency, and durability.[1] The excellent chemical, electronic, and mechanical properties of graphene and its derivatives enable them as alternative materials for fuel cell applications (Figure 1). Great efforts have been devoted to exploiting the potential use of graphene-based materials in the fuel cells in the past few years. Graphene-based materials are ideal electrocatalyst supports, increasing the number of active sites and facilitating the transport of electrons for both fuel oxidation and oxygen reduction reaction (ORR).[2,3] Metal-free graphene

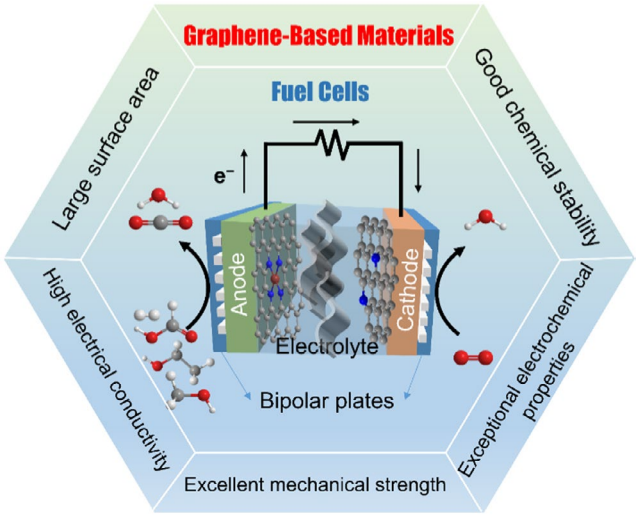

FIGURE 1 Schematic of a fuel cell incorporating graphene-based materials in each component

materials have been demonstrated to be attractive candidates for ORR due to high electrocatalytic activity, high tolerance to poisoning, and low cost.[4] Extensive insights have been obtained to understand the effects of electronic structure modification, doping configurations, defects, or functional groups of graphene on the performance of fuel cells.[4,5] Furthermore, graphene-based materials incorporated in polymer membranes further improve the ionic conductivity and minimize crossover of fuels.[6] Graphene-based materials are promising as proton-exchange membranes with high proton conductivity and impermeability to water, H_2, and methanol.[7] In addition to electrolyte and electrode, graphene-based materials can also improve the current collection, fuel/air distribution, and stability of bipolar plates.[8]

The catalytic and electrochemical properties of graphene-based materials have already been well-reviewed.[9-15] The latest reviews mostly focus on a specific application field related to the fuel cells, including ORR,[3-5] fuel oxidation,[2,16-18] membranes,[6,19] and bipolar plates.[8] Some early comprehensive reviews discussed graphene-based materials and their applications in each fuel cell component, but a summary of the latest developments in this area is still lacked.[20,21] According to the ISI Web of Knowledge search, we found thousands of papers combining the topics of graphene and fuel cells published each year after 2016, which deserve a comprehensive review to keep up to date with the timely progress in this field. This review article summarized the significant roles of graphene-based materials in electrodes, electrolytes, and bipolar plates of fuel cells, emphasizing the recent advancements, including three-dimensional graphene-based electrodes and graphene-supported single-atom electrocatalysts. The key factors that affect the performance of these graphene-based materials in fuel cells were analyzed thoroughly. The underlying mechanisms and design strategies were discussed extensively. Their limitations and future research prospects were also outlined at last.

2 | PROPERTIES OF GRAPHENE-BASED MATERIALS

Graphene is a one-atom-thick layer with sp^2 hybridized carbons in a hexagonal arrangement.[11] The Nobel Prize in Physics in 2010 was awarded to Andre Geim and Konstantin Novoselov for their groundbreaking contributions to the graphene based on their pioneering work in 2004.[22] Since then, graphene has become the fastest-growing science branch, which stimulated great efforts and made significant progress in this area. Graphene-based materials contain not only graphene, but also graphene oxide (GO), reduced graphene oxide (rGO), heteroatom-doped graphene, functionalized graphene, and three-dimensional (3D) graphene. They exhibit various physical and chemical properties, such as large specific area, excellent electrical and thermal conductivity, high mechanical strength, and good chemical stability (Figure 2).[9-13] These unique properties of graphene and its derivatives make them potentially suitable for fuel cell applications.

2.1 | Properties of graphene

Graphene has a large theoretical surface area of 2630 $m^2\ g^{-1}$, which is about two orders of magnitude larger than that of graphite powder (~10 $m^2\ g^{-1}$).[10] The two-dimensional (2D) morphology of graphene-based materials with the large surface area may have strong adsorption capacity to the reactants by strong interactions with π electrons, allowing to use them as catalysts or catalyst supports.[11] Graphene is a zero-gap semiconductor with high carrier mobility (~10 000 $cm^2\ V^{-1}\ s^{-1}$ at relativistic speed ~10^6 $m\ s^{-1}$) due to the overlap between valence and conductance bands.[22] The mobilities of graphene are less influenced by temperature; hence, the ultrahigh mobility can be achieved at room temperature.[9] The unique electrical properties make the transfer of electronic density between π system of graphene and the substrates more favorable.[11] The twisted bilayer graphene with a magic angle exhibits a special electronic structure with the vanishing of the Fermi velocity at the Dirac points.[23] Furthermore, the good thermal conductivity (~5000 $W\ m^{-1}\ K^{-1}$ for a mechanically exfoliated monolayer graphene) of graphene benefits the application that required strict heat management and the reactions exhibiting a strong endo- or exothermicity.[9] Graphene exhibit a fast-heterogeneous electron transfer (HET) rate and the HET rate at edge planes of graphene is faster than basal or defect-free planes due to the high density of electroactive sites at edges.[10,12] In addition, graphene has good mechanical properties and high thermal stability. Defect-free graphene

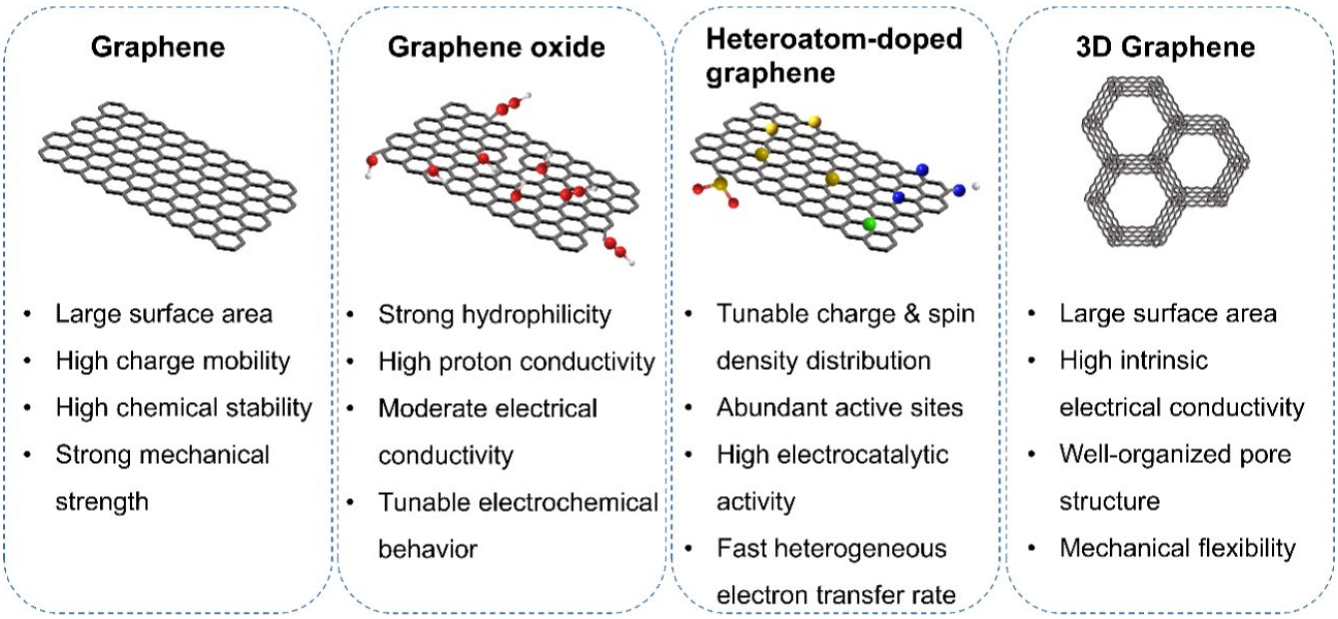

FIGURE 2 The main properties of graphene-based materials are related to fuel cell applications

has a high Young's modulus (~1.0 TPa) and a high fracture strength (~130 GPa).[9] Graphene can resist oxidation up to 300°C based on thermogravimetric measurements.[11]

2.2 | Properties of GO

GO is a single-layer of graphite oxide that is usually produced by the chemical oxidation of graphite.[13] Oxygen functional groups, including hydroxyl and epoxy groups, were identified on the basal plane, while carboxy, carbonyl, phenol, lactone, and quinone groups were mostly formed at the sheet edges.[13] These oxygen-containing groups and defects in GO strongly affect its electronic, electrochemical, and mechanical properties. The electrical conductivity of GO or rGO is several orders lower than the pristine graphene due to the disruption of the sp^2-hybridized carbon network by defects and oxygen-containing groups.[13] The charge-carrier mobility of rGO is reduced to only around 1 $cm^2\ V^{-1}\ s^{-1}$.[24] The presence of a large amount of oxygen functional groups can also lower the HET rate.[12] It was observed that the HET rate increases with increasing C/O ratio of GO and rGO. However, parts of these oxygen functional groups are electrochemically active that can be reduced or oxidized, such as hydroxide, epoxide, peroxide, and carbonyl (aldehyde and quinone) groups. The electrochemical behavior of GO can be tuned by adjusting oxygen functionalities on graphene surfaces. For example, carbonyl groups exhibit stronger reductive overpotentials than epoxide, peroxide, or aldehyde groups, whereas quinone-hydroquinone pair can introduce reversible electrochemical character.[12] Furthermore, GO is strongly hydrophilic and disperse uniformly in water, which renders it as excellent electrode materials.[6,13] GO has a relatively high proton conductivity (1.1×10^{-5}-2.8×10^{-3} S cm^{-1}), suggesting that it is potentially applicable as proton electrolyte in fuel cells.[25] However, GO is vulnerable to high temperatures in the presence of oxygen or reducing reagents, making it only suitable for low-temperature fuel cell applications.[11]

2.3 | Properties of heteroatom-doped graphene

The flexible carbon backbone of graphene provides infinite possibilities for modification and functionalization. Doping heteroatoms (eg, nitrogen, boron, sulfur, halogens, or transitional metals) into both the basal plane and reactive edges of graphene is an effective strategy to tune its electrochemical and catalytic properties. The electron-withdrawing or electron-donating effects and additional structural defects of dopants can alter its electronic properties.[12] These dopants also change the density of state (DOS) near the Fermi energy level and subsequent conductivities of graphene-based materials. Furthermore, the change in spin density distribution and atomic charge distribution due to heteroatom doping increases active sites of graphene and enhances catalytic activity significantly.[14]

Nitrogen is the most popular dopant into graphene. The nitrogen dopants have various moieties, including quaternary-N, pyridinic N, pyrrolic N, amino, and nitrogen oxide.[12,14] The quaternary-N, also called graphitic N, is the doping N atom that is combined into a hexagonal ring. Pyridinic and pyrrolic N form sp^2 and sp^3 hybridized bonds by donating one and two p electrons to the π system, respectively. Nitrogen has a higher electronegativity value (3.04) compared to carbon atoms (2.55), leading to a positive charge density on the

surrounding carbon atoms. The DOS near the Fermi energy level was suppressed by substitutional nitrogen, resulting in bandgap opening.[12] N-doped graphene also exhibits higher HET rates for $Fe(CN)_6^{3-/4-}$ probes.[26] Moreover, N-doped graphene is more stable against chemical oxidation.[11] However, the carrier mobilities and conductivity of N-doped graphene are lower than pristine graphene due to the hinder effects of dopants and induced defects.[12]

Boron is a p-type electron-withdrawing atom, which is contrast to nitrogen, an n-type electron-donating atom. Boron-doped graphene has high carrier concentration since more holes are introduced into the valence band of graphene.[12] Boron dopants also introduce larger DOS near the Fermi energy level, resulting in high conductivity.[26] Both boryl moiety and amino moiety can increase the work function of doped graphene and lead to a p-type semiconductor behavior.[12]

Sulfur-doped graphene contains sulfate, sulfide (thiophene), and/or sulfonate groups.[12] Sulfonate-rich S-doped graphene has a relatively lower conductivity, while thiophene-rich S-doped graphene has better conductivity and charge transfer ability.[12] The electronic properties of S-doped graphene can be modified by adjusting the amount of introduced sulfur.[11] The singly S-doped graphene is a small-bandgap semiconductor, while doubly S-doped graphene exhibits better metallic properties. Moreover, sulfur dopants improve the electrosorption ability of graphene to the electrolyte ions by lowering its affinity to water.[27]

Despite these doping species, the properties of graphene can also be tuned by hydrogenation processes.[28] The main change of hydrogenated graphene is that the layered sp^2-hybridized carbon atoms are converted to sp^3-hybridized carbon defects. Adjusting the extent of hydrogenation of graphene can tune its semiconducting properties.[12] Furthermore, the partially hydrogenated graphene (~19 atomic %) showed a higher HET than pristine graphene due to the existence of more edge defects.[29] Partial H-decorated graphene leads to the formation of single electrons and high local spin density, benefiting for oxygenated component adsorption.[14]

2.4 | Properties of 3D graphene

One of the main drawbacks of the utilization of graphene for fuel cells is that the graphene sheets tend to restack due to the attractive forces between graphene sheets, leading to a decrease in the availability of active sites. The issues can be well-solved by 3D-structured graphene with a curved non-planar shape and tailored hierarchical porosity.[30] The continuous conductive network provides fast electron transport, and an interconnected hierarchical porosity of 3D graphene is favorable for ion transport.[31] Therefore, 3D graphene presents a faster HET rate than 3D porous carbon,[10] or an enhanced ORR activity when serving as conducting support for electrocatalysts.[32] Moreover, a high mass loading and a more efficient charge transport pathways process throughout the entire frameworks of 3D graphene electrodes can be obtained.[33] 3D graphene has various architectures, such as graphene sphere, graphene fibers, vertical graphene films, graphene networks, graphene cages, etc, leading to diverse electrical, chemical, and mechanical properties.[34,35] For example, the 3D porous graphene fabricated by laser beam reduction of GO has high conductivity (1738 S m^{-1}) and a large specific surface area (1520 m^2 g^{-1}).[36] The Ca^{2+}-cross-linked reduced giant graphene fibers showed an excellent tensile strength of 501.5 MPa and electrical conductivity of 4.1×10^4 S m^{-1}.[37] The 3D cabbage-coral-like graphene has abundant micropores incorporated in the surface layer of the graphene walls with an average diameter of 1.6 nm, which benefits electrolyte ion transport.[38]

3 | SYNTHESIS OF GRAPHENE-BASED MATERIALS

The structures and properties of graphene-based materials are strongly dependent on the fabrication methods. Two approaches are often employed, namely, top-down and bottom-up (Figure 3).[9-12,24] The top-down methods include the mechanical exfoliation, liquid-phase exfoliation, oxidation exfoliation, and electrochemical exfoliation of graphite. The bottom-up approaches synthesize graphene from organic precursors through epitaxial growth on silicon carbide (SiC), chemical vapor deposition (CVD), alkaline metal chemical reactions, or other chemical processes. Generally, the top-down strategy is relatively cost-effective and appropriate for large-scale production, while the bottom-up strategy can produce higher-quality graphene deposited on the substrates.[9-12,24]

3.1 | Synthesis of graphene and GO

3.1.1 | Top-down strategy

The graphene sheets in the graphite are bounded by weak van der Waals forces with an interlayer distance of 3.35 Å. Hence, the single-layer graphene can be obtained by simple mechanical exfoliation using an adhesive tape.[22] This pristine graphene has a low density of defects, but it is not suitable for large-scale production.[10,24]

Liquid-phase exfoliation can facilitate the exfoliation of graphene sheets by organic solvents with certain surface tensions (40-50 mJ m^{-2}) under sonication.[10] This process can be improved by altering external forces (ie, sonication, ball milling, shear mixing) or adding surfactants or polymers.[24] However, the exfoliation efficiency of liquid-phase

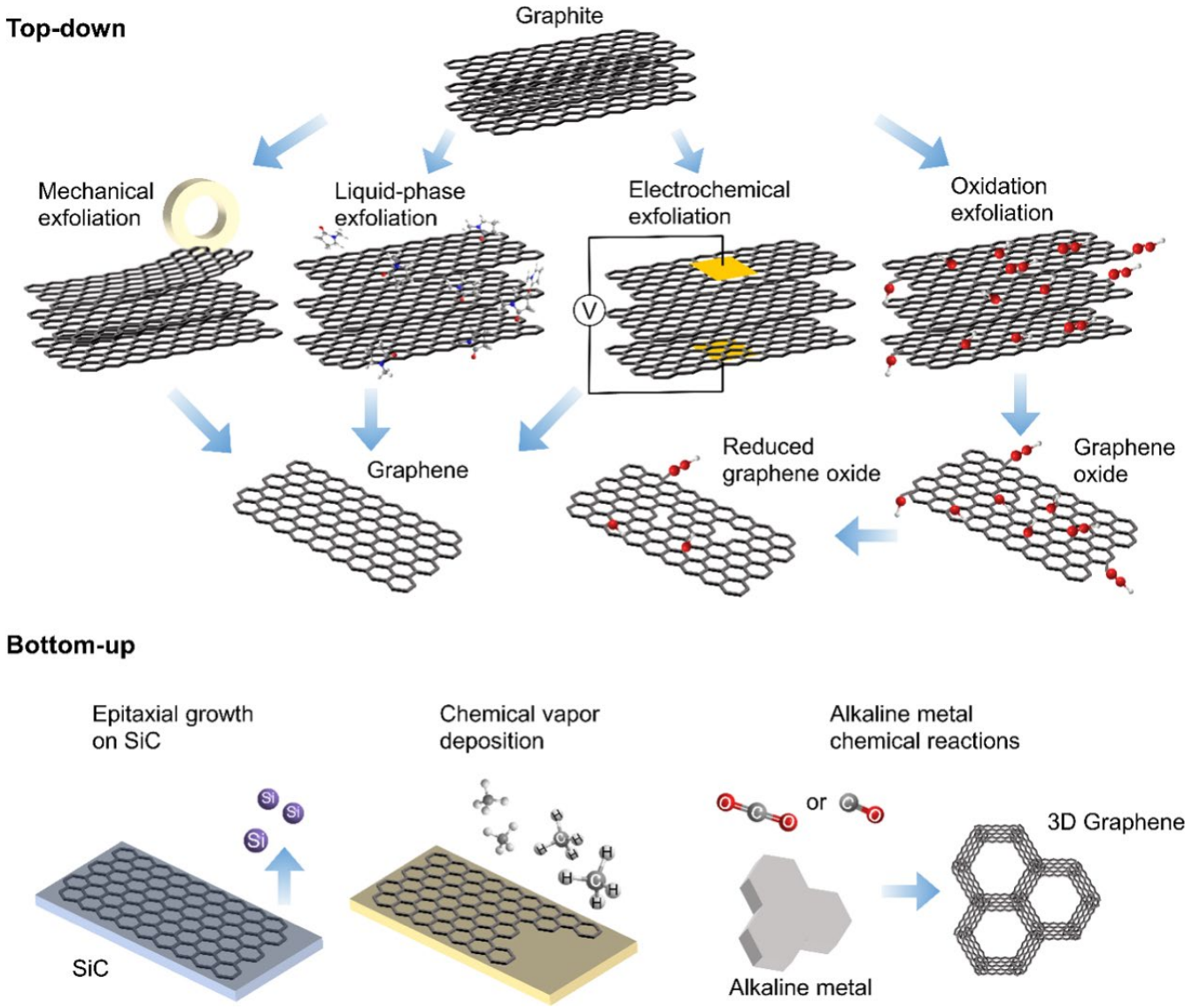

FIGURE 3 Major synthesis methods of graphene

exfoliation is quite low (<1%).[10,24] Great advances have been achieved in microwave irradiation of graphite in molecularly engineered oligomeric ionic liquids, which can produce high-quality graphene (95% selectivity to single-layer graphene) with high yield (93%).[39]

GO fabricated from well-known Hummers method or modified Hummers method via reaction of graphite and potassium permanganate ($KMnO_4$) and concentrated sulfuric acid (H_2SO_4) has achieved wide application.[13] Although this method requires toxic and dangerous chemical agents, it is attractive because it provides an opportunity for mass production of graphene. The rGO can be obtained by further eliminate a majority of oxygen functional groups of GO via chemical reduction, thermal treatment, electrochemical reduction.[9-12,24] The rGO presents improved characteristics than GO due to the residue oxygen-containing groups and abundant defects.[10] Hydrothermal reduction of high concentration (>2 mg mL^{-1}) of dispersed GO followed by freeze-drying can form a 3D self-assembled graphene aerogel.[40] An important approach for reduction of GO was developed to produce high-quality rGO with negligible in-plane oxygen concentrations (~4 at%) and high charge-carrier mobilities (>1000 cm^2 V^{-1} s^{-1}) using a strong microwave (1000 W).[41]

Electrochemical exfoliation of graphite can control the chemical and structural features of graphene and improve graphene yields, which has been considered a promising technique for large-scale production of high-quality graphene sheets.[10,12,24] In the electrochemical process, the anodic (or cathodic) potential is applied to facilitate the intercalation of negative anions (or positive cations) into the graphite layers followed by expansion and exfoliation. The anodic exfoliation is more efficient since the radical species formed by the oxidation of water facilitate the exfoliation process, but the graphene sheets fabricated by cathodic exfoliation have higher quality.[10,12] The graphene synthesized by electrochemical exfoliation is suitable for the use

of polymer membrane fillers that charge-carrier mobilities are not critical.[24] Electrochemical exfoliation is also a green, safe, and fast approach to synthesize GO.[42] The GO properties can be tailed by manipulating raw graphite electrode materials, electrolytes, applied voltages/currents, and operation mode.[42]

3.1.2 | Bottom-up strategy

The CVD growth of graphene sheets on metallic substrates (such as Cu and Ni) from thermal decomposition of carbonaceous sources followed by transfer process and chemical etching is a well-known bottom-up strategy.[43] The properties of CVD graphene strongly depend on the conditions for the growth of graphene.[24] For example, if using a 3D-structured nickel foam as a metallic template, a 3D graphene foam with high conductivity (10 S cm^{-1}) can be obtained.[44] The transfer process of the CVD approach is time-consuming and causes contamination issues. Electrochemical assisted delamination of the CVD graphene is fast, environmentally friendly, and more controllable.[12] For example, the poly(methyl methacrylate) (PMMA)-supported graphene can be delaminated from Cu foil within 1 hour by H_2 bubbles generated under a voltage bias of −5 V.[12]

Graphene growth on SiC under high-temperature (1150°C) and vacuum conditions or a higher temperature (1650°C) in Ar atmosphere is promising for integration in current industrial procedures but limited by the high cost of single-crystal SiC.[24] Graphene can be considered as a polycyclic aromatic hydrocarbon of infinite size; thus, it can be fabricated via organic synthesis routes.[10,24] However, these multistep organic synthesis routes are expensive, and the obtained graphene nanoribbons are limited by size.[10,24]

These aforementioned bottom-up methods are not suitable for bulk-scale graphene production and suffer from high cost and energy consumption.[24] Furthermore, H_2 gas is generally used to pretreat the Cu surface and is mixed with CH_4 during the CVD process, leading to a potential risk of explosion.[24] Hu and coworkers discovered an alkali-metal-triggered redox reaction for mass production of 3D graphene from CO or CO_2.[45-48] Benefiting from the exothermic nature of the reaction and isolation of graphene sheets by in situ formation of alkali metal carbonate nanoparticles, a high yield of well-controlled 3D graphene can be obtained at a lower temperature. Recently, Tour and coworkers invented the flash Joule heating approach to convert various low-cost carbon-containing materials (such as carbon black, biochar, and even daily-life waste) to high-quality graphene within one second.[49,50] Furthermore, the electric energy consumption is only about 7.2 kJ/g graphene, which makes it promising for gram-scale graphene production.

3.2 | Synthesis of graphene-based electrocatalysts

Heteroatom-doped graphene demonstrates unique catalytic activities, especially for ORR.[5,11,18] Numerous technologies were exploited to introduce foreign atoms into graphene, such as CVD, thermal annealing, hydrothermal treatment, ball milling, and plasma treatment.[5,11,18] CVD is a kind of in situ doping process using heteroatom-containing precursors besides carbon-containing sources. The N-doped graphene grown on nickel substrate fed with a gas mixture (NH_3:CH_4:H_2:Ar = 10:50:65:200) has been applied for the cathode in alkaline fuel cells and showed a superb performance than commercial Pt/C.[51] Thermal annealing of a mixture of GO and various doping precursors is a simple approach to synthesize single-doped or co-doped graphene. A quaternary-doped graphene has been successfully prepared using GO, boric acid, melamine, dibenzyl disulfide, and orthophosphoric acid under 900°C and N_2 atmosphere.[52] Zeolitic imidazolate frameworks (ZIFs) with 2D crystal structures are attractive precursors to prepare heteroatom-doped graphene with high porosity and rich active sites.[53] In the synthesis process, Zn-containing ZIF nanoleaves was thermally exfoliated by metal chlorides under an inert atmosphere, followed by acid washing (Figure 4). Hydrothermal reduction of GO is a green method for heteroatom-doped graphene synthesis without using hazardous reducing agents.[18] Chai et al[54] developed an one-pot hydrothermal reaction for the synthesis of P, N co-doped graphene using GO with diammonium phosphate or ammonium dihydrogen phosphate as phosphorus and nitrogen precursors. By further introducing cyanamide for additional nitrogen doping, the ORR activity of P, N co-doped graphene outperformed Pt/C due to the modulation or P-N bond and graphitic N. Ball milling is an energy-saving synthesis method that reduces the activation energy of reactions.[5] Jeon et al[55] selectively incorporated S into the edge of graphene nanoplatelets using a ball-milled approach. The highly improved ORR activity was attributed to the high electronic spin density of sulfur oxides (O=S=O) doped at the edges of the graphene.

Graphene is an idea electrocatalyst support due to its large surface area, high electric conductivity, and high electrochemical stability.[11,18] Various physical or chemical approaches were explored to anchor metal or metal oxide on the graphene support, such as chemical reduction process, thermal treatment, hydrothermal or solvothermal processes, self-assembly, and electrochemical processes.[13,15,18] Chemical reduction is a common way to prepare graphene-supported metal catalysts using various reducing agents, including sodium borohydride ($NaBH_4$), sodium citrate, ethylene glycol (EG), and GO (or rGO).[18] Perivoliotis et al[56] prepared Pd@Ni/S-doped graphene by a modified polyol reduction method. The S-doped graphene was prepared using diethylene glycol

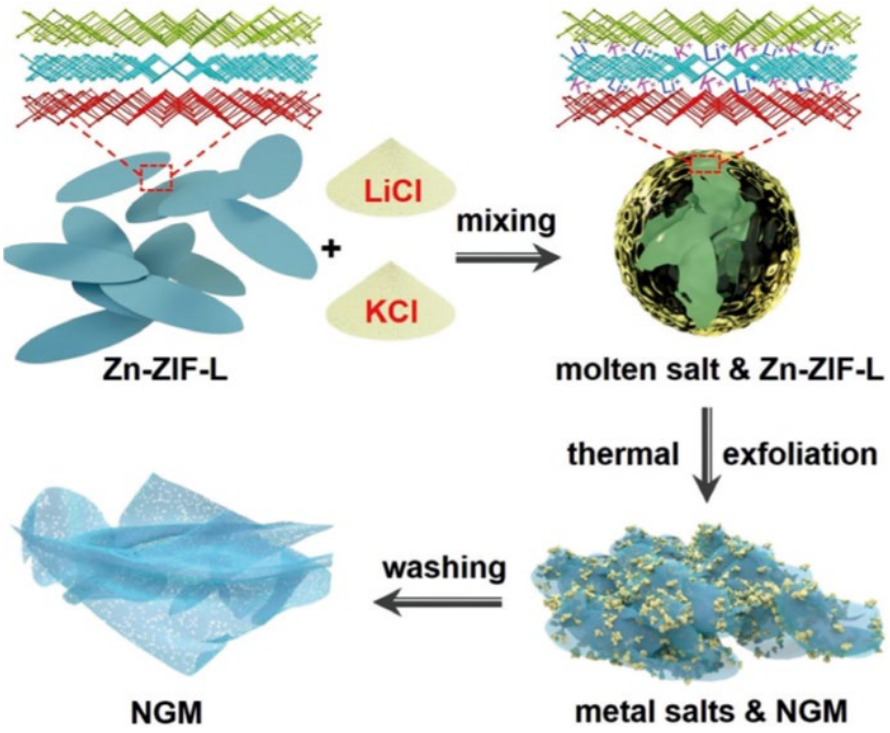

FIGURE 4 Schematic illustration of the synthesis of N-doped graphene nanomesh (NGM) from Zn-containing ZIF nanoleaves (Zn-ZIF-L). Reprinted with permission from Ref.[53] Copyright 2019 John Wiley and Sons

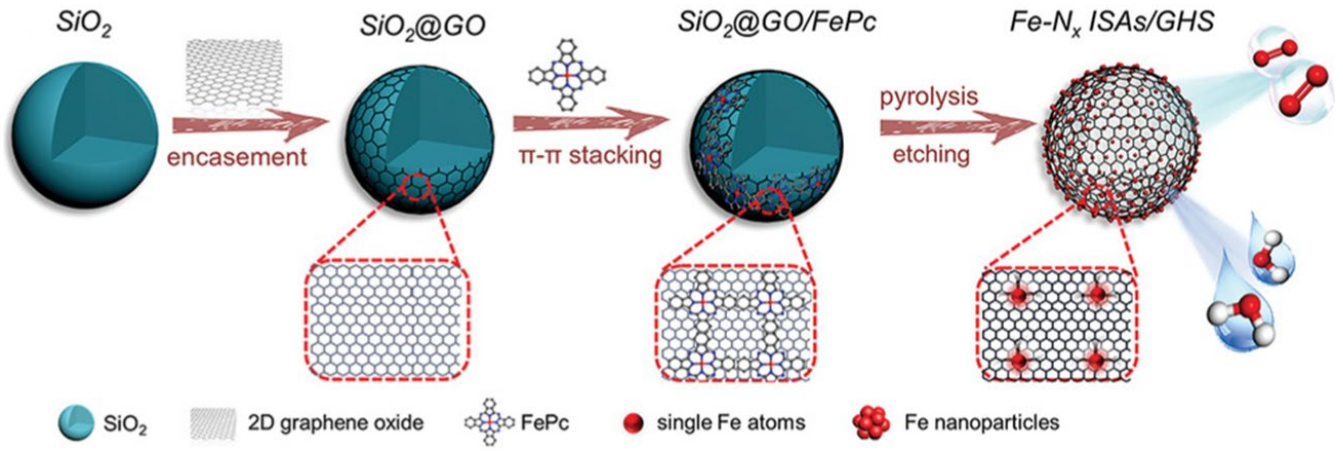

FIGURE 5 Schematic illustration of the synthesis of isolated Fe single atomic sites anchoring graphene hollow nanospheres (Fe ISAs/GHSs) using Fe phthalocyanine (FePc) as iron precursors. Reprinted with permission from Ref.[59] Copyright 2019 John Wiley and Sons

methyl ether as a solvent and Lawesson's reagent as a sulfur source. Then, $NaBH_4$ dissolved in EG was gradually added into a mixture of nickel acetate tetrahydrate and S-doped graphene, followed by deposition of a Pd shell via the galvanic replacement method using potassium tetrachloropalladate (K_2PdCl_4). GO or rGO support processes self-reducing ability and metal precursors can be directly reduced on GO or rGO nanosheets. For example, a Pt-Pd nanoflowers/GO can be obtained by simply mixing GO, potassium tetrachloroplatinate (K_2PtCl_4), and sodium tetrachloropalladate (Na_2PdCl_4) in ethanol solutions for 1 hour at room temperature.[57] Thermal treatment of metal and graphene precursors is a facile and general approach to fabricate graphene-supported electrocatalysts. Recently, Cheng et al[58] developed one-pot pyrolysis to synthesize single iron atoms on graphene using hemin porcine and dicyandiamide as precursors. The mixture was annealed at 350°C and 650°C in Ar for 3 hours, followed by heat treatment at 900°C in Ar for 1 hour. Another isolated Fe single atomic sites anchoring graphene hollow nanospheres (Fe ISAs/GHSs) was synthesized by a template-assisted thermal pyrolysis method using SiO_2 nanospheres as templates and Fe phthalocyanine as Fe precursors (Figure 5).[59] The Fe ISAs/GHSs can be obtained by thermal reduction at 700°C in an N_2 atmosphere. Liu et al[60] designed a solvothermal approach that allowed the one-pot fabrication of Pt-Cu/GO. In the work, platinum(II) acetylacetonate, copper(II)

acetylacetonate, sodium iodide, and poly(vinyl pyrrolidone) were dissolved in N,N-dimethylformamide, and then mixed with hydroxylamine hydrochloride and GO, followed by solvothermal treatment at 130°C for 8 hours. Yamauchi et al[61-63] synthesized various graphene-supported electrocatalysts from the self-assembly of block copolymer micelles and metal salts and then carbonation. The obtained metal nanoparticles/N-doped graphene hollow spheres showed superior ORR activity and stability than commercial 20 wt.% Pt/C catalysts due to the well-distributed metal nanoparticles and porous hybrid architectures. Electrodeposition is a controllable and template-free approach to synthesize graphene-supported electrocatalysts. Wang et al[64] prepared Pt-Ni/porous rGO using a two-step approach. In the synthesis process, GO was firstly treated by $KMnO_4$, hydrogen peroxide (H_2O_2), and hydrochloric acid (HCl) and deposited on a glassy carbon electrode. Pt-Ni nanoparticles were then electrodeposited on the electrode surface using hexachloroplatinic acid (H_2PtCl_6) and nickel sulfate ($NiSO_4$) precursors. Ren et al[65] developed an environmentally friendly and surfactant-free approach to synthesize Pt-Pd/rGO. In this case, a mixture of $PtCl_6^{2-}$, $PdCl_4^{2-}$, and GO were firstly reduced by H_2, followed by electrochemical reduction under the cathodic bias of −0.9 V.

3.3 | Synthesis of graphene-based membranes

The high proton conductivity, good chemical stability, and excellent mechanical properties of GO render it an ideal filler material for polymer membranes of fuel cells. Two approaches are frequently used to fabricate GO-polymer composite, namely, in situ intercalative polymerization and solution intercalation.[13] In the in situ intercalative polymerization process, GO is mixed with liquid monomer precursors, and then the polymerization is initialized by an initiator under controlled conditions. Epoxy and polyaniline (PANI) are typical polymers that coupled with graphene by in situ polymerization. For example, a PANI/rGO membrane can be prepared by mixing ammonium peroxydisulfate, aniline monomer, and GO in the acidic aqueous solutions, and then reduced by hydrazine.[66] In the solution intercalation process, the well-dispersed soluble polymer and GO were reassembled to form a composite with the aid of sonication or mechanical mixing. This approach is straightforward and frequently used for the preparation of GO-polymer composites. For example, a poly(vinyl alcohol) (PVA)/graphene membrane was fabricated by mixing the water-soluble PVA and GO under mechanical stirring, followed by hydrazine reduction and film casting (Figure 6).[67] Similar approaches were also exploited for the preparation of Nafion/GO[68,69] and sulfonated poly (ether ether ketone) (SPEEK)/sulfonated GO[70,71] with the assistance of organic solvent. However, the low solubility of GO and rGO in organic solvents may lower the dispersity of the filler, thus the content of GO fillers and mixing conditions should be carefully adjusted. The properties of the GO-polymer composite membrane are also dependent on the bonding between the graphene and the polymer matrix. To improve the compatibility between the matrix and the fillers, Liu et al[72] prepared a quaternized graphene by hydrothermal treatment of (3-Aminopropyl)triethoxysilane (APTES)-functionalized graphene and the subsequent epoxide-ring opening reaction. The quaternized graphene was then incorporated into quaternized polysulfone (QPSU) via a blending method.

Apart from the synthesis of GO-polymer composite, GO can be directly used as proton electrolyte in fuel cells due to

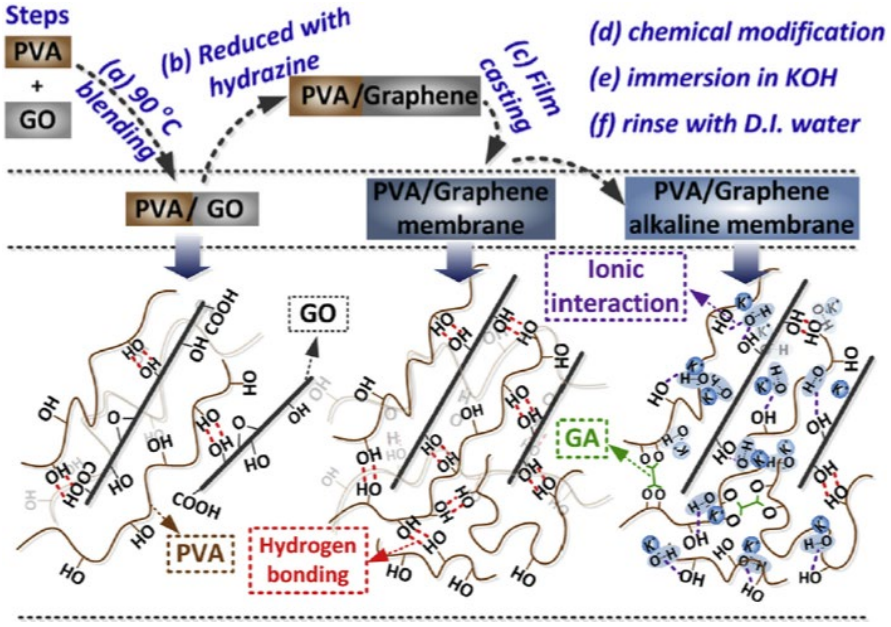

FIGURE 6 Schematic illustration of the PVA/graphene composite membrane synthesis procedure. Reprinted with permission from Ref.[67] Copyright 2013 Elsevier

its higher proton conductivity and low permeability to reactant species.[73] A simple vacuum filtration approach can be used to fabricate a GO paper from well-dispersed GO solution.[74] For example, a 22 μm-thick ozonated GO film was obtained by bubbling O_3 gas of 5 mg mL^{-1} GO solution, followed by vacuum filtration through a 0.22 mm cellulose membrane.[75] Furthermore, layer-by-layer assembling was conducted to fabricate graphene on the membrane electrode assembly (MEA). Holmes et al[76] coated single-layer graphene on the MEA of a direct methanol fuel cell (DMFC) by the CVD approach. The CVD grown graphene layer on Cu was spin-coated with PMMA. After etching the Cu by ammonium persulfate, the floating graphene-PMMA layer was transferred onto the MEA in a water bath. In another case, Nafion ionomer was spin-coated on the graphene/copper surface, followed by transferring onto a Nafion 212 membrane.[77] Another Nafion 212 membrane was hot-pressed onto graphene film to fabricate a Nafion | graphene | Nafion sandwiched structure.

4 | GRAPHENE-BASED MATERIALS FOR FUEL CELL APPLICATIONS

Many advantages have been demonstrated for the applications of graphene materials as active components of fuel cells. The high surface area and high conductive properties of graphene-based materials are promising to use as electrocatalysts for ORR and fuel oxidation. The polymer membranes combined with graphene possess high ionic conductivity, high tensile strength, and low fuel permeation. Graphene can enhance the conductivity and corrosion resistance of bipolar plates. Table 1 summarized representative graphene-based materials for various fuel cell applications.

4.1 | Graphene-based cathodes

The electrochemical reaction of fuel cells is determined by ORR at the cathode. The sluggish ORR kinetics requires high-cost platinum catalysts. Furthermore, the platinum catalyst is sensitive toward CO poisoning, which hinders its application. Therefore, various alternative graphene-based materials have been explored for ORR, not only as supports for metal nanoparticles, but also directly as metal-free electrocatalysts.

4.1.1 | Graphene-supported ORR electrocatalysts

Conductive graphene-based materials are usually utilized as supports for metal nanoparticles to facilitate electrons transfer to the electrode surface. For example, N-doped graphene support was found promoting the dispersion and durability of Pt-Co alloy nanoparticles by increasing nucleation and growth kinetics of nanoparticles and support/catalyst chemical binding.[78] The PEMFC with Pt-Co/N-doped graphene cathode showed a four times higher maximum power density (805 mW cm^{-2} at 60°C) than that with commercial Pt/C cathode. Platinum group metal-free (PGM-free) catalysts are more promising for large-scale commercialization. Liang et al[79] reported that Co_3O_4/rGO composite exhibits similar catalytic activity with an ORR onset potential (E_{onset}) of about 0.83 V vs reversible hydrogen electrode (RHE), but superior stability (little decay in ORR activity over 25 000 seconds) to Pt in alkaline solutions. Its superb activity was attributed to synergetic chemical coupling effects between the metal oxide and graphene.

The 3D graphene has large surface area and porosity, excellent electrical conductivity, and interconnected pore structures, not only providing more anchor sites to immobilize metal oxide nanoparticles but also improving the mass transport of reactants.[80,81] Hu and coworkers collaborated with other groups to explore their 3D honeycomb-structured graphene (HSG) for ORR by developing the novel Pt-Fe/HSG electrode with a modified supercritical fluid technique.[80] A high mass activity of 1.70 A mg_{Pt}^{-1} was achieved for $Pt_{40}Fe_{60}$/HSG, which was 14.2 times higher than that of commercial Pt/C (0.12 A mg_{Pt}^{-1}). Furthermore, they prepared Fe/N/S incorporated Fe_3O_4 nanoparticles on 3D HSG (Fe_3O_4/FeNSG-3) as PGM-free ORR catalysts using melamine formaldehyde resin as a soft template and nitrogen source.[81] The as-prepared catalyst exhibited a much more positive E_{onset} (0.951 V vs RHE) than that (0.923 V vs RHE) of commercial Pt/C in alkaline media, which was attributed to the 3D porous structures, abundant active sites and larger surface area (530.5 m^2 g^{-1}). Moreover, the Fe_3O_4/FeNSG-3 maintained 71.5% of the initial current after 30 000 seconds continuous operation, demonstrating higher durability than the Pt/C catalyst (54.4% of the initial current remained).

Heteroatom-doped and defective graphene can be used as ideal supports to anchor a single metal atom.[82] These graphene-supported single-atom catalysts (SACs) exhibited high ORR activity and selectivity for the four-electron reaction route, as well as long-term stability in alkaline or acidic conditions (Table 2). Their superior performances were attributed to the high density of active sites, the strong interactions between individual atoms and graphene supports, and the charge redistributions in the graphene support.[82] For example, Zhang et al[83] reported that atomically dispersed Ru on N-doped graphene exhibited higher ORR activity, better durability, and tolerance toward methanol and CO poisoning than commercial Pt/C catalyst in 0.1 mol/L $HClO_4$. Shu et al[84] dispersed single-atom Co species on to sulfuric acid-treated N-doped graphene, demonstrating higher durability (94% of the initial current density

TABLE 1 Representative work of graphene-based materials for applications of fuel cells

Applications	Graphene-based materials	Performances	Mechanisms	Ref
ORR in alkaline	N-doped graphene	Activity is 3 times higher than that of Pt/C	Nitrogen atom creates positive charge on adjacent carbon atoms and acts as active sites	51
	Edge-sulfurized graphene	High ORR electrocatalytic activity, better fuel selectivity and a longer-term stability than those of Pt/C	Sulfur atoms and sulfur oxides at the graphene edges increase the spin and charge densities	55
	Co_3O_4/N-doped graphene	Similar catalytic activity but superior stability to Pt/C	Synergetic chemical coupling effects between Co_3O_4 and in graphene	79
ORR in acid	N-doped graphene	Activity increases with increasing concentration of pyridinic N	The Lewis base site created by pyridinic N is the active site for ORR	108
	Fe-N-rGO	Higher mass activity and improved stability than the Fe-N-C	Synergetic effects of Fe-N_3 moiety, abundant pyridinic N, and higher degree of graphitization	97
MOR	Pt/graphene nanosheets	Higher activity and CO tolerance than Pt/C	Modulation in the electronic structure of the Pt clusters (~0.5 nm)	116
	Pt/N-doped graphene	Enhanced the MOR activity compared with Pt/graphene	The nitrogen functional groups and the uniform distribution of Pt particles on the doped graphene	118
	Ni/rGO	Higher mass activity (1600 mA mg^{-1}) and stability (maintains 1012 mA mg^{-1} after 1000 cycles) than Pt/C	The ultrafine size (~2.3 nm) and high dispersity of Ni nanoparticles on rGO	120
EOR	PtPd (1:3)/rGO	Superior catalytic activity than the monometallic Pt or Pd catalyst	Synergistic effect between Pt and Pd and the ligand effect	65
	PtRh nanowire/graphene nanosheets	A 5.4-fold mass activity compared to Pt/C	Synergistic effects of one-dimensional PtRh alloys and graphene nanosheet support	130
Anode in MFCs	Oriented rGO/polyacrylamide/graphite brush	An activation polarization resistance of 4.4 Ω cm^{-2} and a maximum power density of 782 mW m^{-2} in 1 g L^{-1} sodium acetate	High surface area, high electron conductance, and high affinity to microbial biofilms	143
	rGO/*S oneidensis* MR-1 hybridized biofilm on carbon cloth	A charge-transfer resistance of ~750 Ω and a maximum power density of ~843 mW m^{-2} in 18 mmol/L lactate	High biomass loading and enhanced direct contact-based extracellular electron transfer	139
Electrolytes	GO membrane for a H_2/O_2 fuel cell	A proton conductivity of 10^{-6}-10^{-4} S cm^{-1} at relative humility of 10%-20% and a peak power density of ~13 mW cm^{-2} at 25°C	High proton conduction and H_2 and O_2 gas impermeability	73

(Continues)

TABLE 1 (Continued)

Applications	Graphene-based materials	Performances	Mechanisms	Ref
	Graphene/Nafion 117 membrane for DMFC	A methanol permeability of 2.19×10^{-6} cm^2 s^{-1} in 1 mol/L CH_3OH and a maximum power density of 75 mW cm^{-2} at 70°C	Graphene provides tortuosity for the methanol without affecting the proton conductivity	76
Bipolar plates	Multilayer graphene/Ni foam	Corrosion rate is two-order-of-magnitude than that of bare Ni foam with a maximum power density of 967 mW cm^{-2}	High chemical durability and conductivity of graphene as a highly efficient corrosion barrier	152
	GO/Polypyrrole/stainless steel 304	Highly stable in 0.1 mol/L H_2SO_4 for 648 h	GO/Polypyrrole coating provides effective physical barrier with the sustained anodic protection	155

Abbreviations: DMFC, direct methanol fuel cell; EOR, ethanol oxidation reaction; FAOR, formic acid oxidation reaction; MFC, microbial fuel cell; MOR, methanol oxidation reaction; ORR, oxygen oxidation reaction; rGO, reduced graphene oxide; RHE, reversible hydrogen electrode.

remained after 7200 seconds operation in 1 mol/L methanol) than that (87% remained) of Pt/C due to the strong covalent bonding between CoN_x species and graphene. Mou et al[85] reported that the ORR active sites on atomically dispersed Cu atoms confined in N-doped graphene are a mixture of Cu-N_2 and Cu-N_4 moieties. Furthermore, Guan and coworkers immobilized various atomically dispersed metals in N-doped graphene lattices by a facile annealing strategy for ORR, such as Co,[86] Fe,[87] Cu,[88] Mn,[89] Sc,[90] Rh,[91] and Ru.[92] In the synthesis process, a certain amount of metal salts and GO were well dispersed in water by sonication, and then water was removed by rotary evaporator. The graphene-based SACs were obtained via a subsequent thermal pyrolysis process under NH_3 atmosphere.

Among these graphene-supported SACs, the iron and nitrogen co-doped graphene (Fe-N-G) catalysts have received tremendous interests due to their high activity and stability for ORR, as well as low cost.[58,59,87,93-95] The iron atomically disperses over the pyridinic nitrogen-containing in-plane or edge defects in graphene to form various active moieties, such as Fe-N_4, Fe-N_{2+2} (bridging between two carbon crystallites), pyridinic N, pyrrolic N, metallic iron and iron carbides.[96] Progresses have been made to identify the possible active sites in Fe-N-G for ORR. For instance, the active sites for ORR of a Fe-N-G catalyst prepared by heat treatment of iron salts, graphitic carbon nitride (g-C_3N_4), and rGO was ascribed to pyridinic N and Fe-N_{2+2} moiety.[97] The single Fe atom catalyst prepared by one-step ball milling of iron phthalocyanine and graphene nanosheets (GNS) showed higher stability and resistance to SO_x, NO_x, and methanol than Pt/C due to the confinement effect of unsaturated Fe centers by GNS via four N atoms.[98] Furthermore, the catalytic sites for ORR in the NH_3-pyrolysed iron- and nitrogen-doped graphene materials were identified by Zitolo et al[99] based on Mössbauer spectra and X-ray absorption near-edge spectroscopy (XANES) spectra. They found that the Fe atoms in the FeN_4C_{12} moieties formed in disordered graphene sheets or zigzag graphene edges were responsible for chemisorption of O_2 molecule and weakening the O–O bond. In another study, the Fe-N_4 moieties near the edge of the graphene layers dominated the ORR activity of a Fe-N-G catalyst prepared by iron salts, cyanamide, and polyaniline based on atomic-resolution scanning transmission electron microscopy (STEM).[100] The identification of active sites would benefit rational designing efficient atomically iron dispersed graphene-based catalysts for ORR.

Density functional theory (DFT) calculations were employed to investigate structure-activity relationships for graphene-supported SACs. Xu et al[101] proposed a descriptor (φ) that relates to valence electrons in the *d* orbital of the metal atom, coordination number, and electronegativity of the metal and neighboring atoms of graphene-supported SACs. The descriptor φ correlated well with adsorption free energies of OH^* (ΔG_{OH^*}) and theoretical/experimental E_{onset} for ORR, indicating φ is a well-defined predictor for ORR activity (Figure 7). It was found that Fe-pyridine-N_4, Fe-pyrrole-N_4, Au-SV-C_3, and Tc-pyrrole-N_4 on graphene support are promising SACs for ORR. Xiao et al[102] reported that graphene-supported-Ir SAC has a faster theoretical ORR kinetics than graphene-supported Mn, Fe, and Co SACs since it is more energetically favorable binding with intermediate species. Furthermore, single-site Ni supported on pentagon | octagon | pentagon graphene demonstrated lowest theoretical overpotential of 0.62 V for ORR among six transition metals (Ni, Cr, Mn, Fe, Co, and Cu).[103]

4.1.2 | Graphene-based metal-free ORR electrocatalysts

Graphene-based metal-free catalysts can address the metal leaching and metal-ion contamination issues caused by

TABLE 2 ORR performance of the graphene-supported single-atom catalysts (SACs)

Graphene-based SACs	E_{onset}, V vs RHE	$E_{1/2}$, V vs RHE	Electron transfer number	Durability	Electrolyte	Ref
Fe@NG-750	1.03	0.90	~4.0	1.6% loss in 25 000 s	0.1 mol/L KOH	87
Fe@NG-750	0.83	0.72	NA	<9% loss in 14 h	0.5 mol/L H_2SO_4	87
Fe–N_x ISAs/GHS	1.05	0.87	~4.0	27.2% loss in 12 000 s	0.1 mol/L KOH	59
Fe_1-N-NG/rGO	0.96	0.84	~4.0	<5 mV loss in $E_{1/2}$ after 15 000 cycles	0.1 mol/L $HClO_4$	93
FeSA-G	0.950	0.804	3.8-3.9	20 mV loss in $E_{1/2}$ after 5000 cycles	0.1 mol/L $HClO_4$	58
SA-Fe/NG	NA	0.88	3.83-3.97	9 mV loss in $E_{1/2}$ after 5000 cycles	0.1 mol/L KOH	94
SA-Fe/NG	0.9	0.8	~3.94	~8 mV loss in $E_{1/2}$ after 5000 cycles	0.5 mol/L H_2SO_4	94
Fe-N-C/rGO	0.94	0.81	3.8-4.0	7.2% loss in 13 000 s	0.1 mol/L KOH	95
Co@NG-750	0.97	0.87	~4.0	6.5% loss in 25 000 s	0.1 mol/L KOH	86
Co@NG-750	0.79	0.69	NA	<1% loss in 50 000 s	0.5 mol/L H_2SO_4	86
Co-N/GS	0.89	NA	3.4	6% loss in 7200 s	0.1 mol/L KOH	84
0.7%Cu@NG-750	~0.94	0.84	4.0	4.0% loss in 25 000 s	0.1 mol/L KOH	88
0.7%Cu@NG-750	NA	0.551	NA	0.7% loss in 13 h	0.1 mol/L $HClO_4$	88
Cu_1/N-Graphene	0.869	0.779	~3.8	NA	0.1 mol/L KOH	85
Mn@NG	0.95	0.82	~3.86	~12.7% loss in 14 h	0.1 mol/L KOH	89
Sc@NG-750	0.99	0.89	~3.9	<2% loss in 50 000 s	0.1 mol/L KOH	90
Sc@NG-750	0.82	0.72	~4.0	5.8% loss in 50 000 s	0.5 mol/L H_2SO_4	90
Rh@NG	NA	0.848	3.82-4.0	12.5% loss in 25 000 s	0.1 mol/L KOH	91
Rh@NG	0.85	0.74	~4.0	3.9% loss in 25 000 s	0.1 mol/L $HClO_4$	91
0.4-Ru@NG-750	0.945	0.826	3.8	<5.7% loss in 25 000 s	0.1 mol/L KOH	92
0.4-Ru@NG-750	0.893	0.723	~4.0	~22% loss in 50 000 s	0.1 mol/L $HClO_4$	92
Ru-N/G-750	0.89	0.75	~3.9	10% loss in 10 000 s	0.1 mol/L $HClO_4$	83

metal-based catalysts.[4] Qu et al[51] explored N-doped graphene as a non-metal electrocatalyst for ORR. Namely, they prepared the N-doped graphene with ~4 at% N/C ratio with the CVD approach, exhibiting 3 times higher steady catalytic current density than commercial Pt/C electrode in 0.1 mol/L KOH. Sun et al[104] reported an ultrathin N-doped holey carbon layer on GNS, which showed excellent ORR performance (E_{onset} = 0.80 V vs RHE; $E_{1/2}$ = 0.65 V vs RHE) in 0.5 mol/L H_2SO_4. Intensive efforts were made to understand the catalytic mechanisms and the active sites of N-doped graphene for the ORR activity. Geng et al[105] attributed the improved ORR activity of N-doped graphene to graphitic N based on the observation of matching relationship between activity and graphitic N contents. Lai et al[106] found that both graphitic and

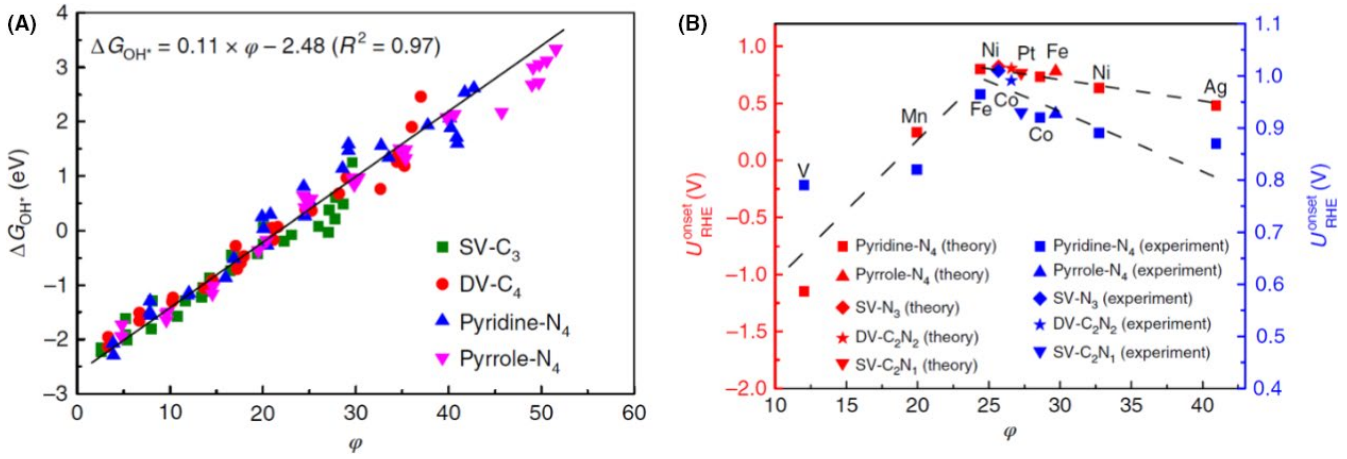

FIGURE 7 (A) Adsorption free energy of OH^* (ΔG_{OH^*}) vs the descriptor φ. (B) Theoretical and corresponding experimental E_{onset} for ORR vs the descriptor φ for single metal atoms supported on graphene. Four coordination environments were considered, including single vacancy with three atoms (SV-C_3), double vacancy with four carbon atoms (DV-C_4), four pyridine N atoms (pyridine-N_4), and four pyrrole N atoms (pyrrole-N_4). Reprinted with permission from Ref.[101] Copyright 2018 Springer Nature

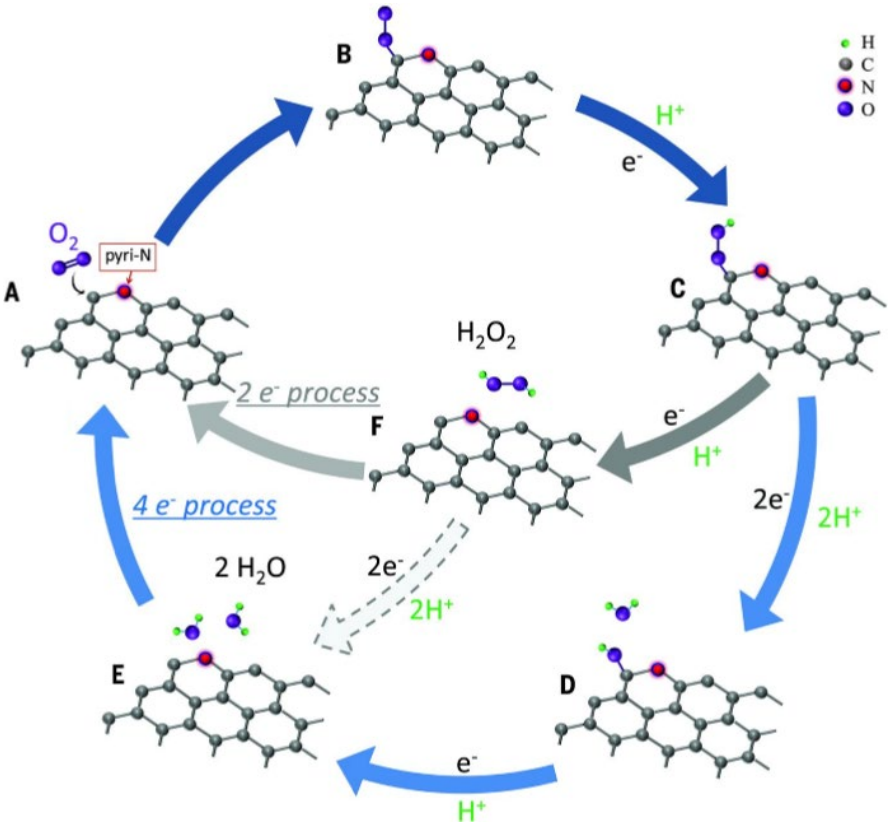

FIGURE 8 Schematic pathways for oxygen reduction reaction on N-doped graphene. Reprinted with permission from Ref.[108] Copyright 2016 The American Association for the Advancement of Science

pyridinic nitrogen were demonstrated as active sites for ORR. Specifically, the graphitic N determined the limiting current density, whereas the pyridinic N enhanced the onset potential for ORR. Moreover, pyridinic-N-rich graphene was observed being selective toward the four-electron pathway of ORR in alkaline solutions.[107] Recently, Guo et al[108] determined that the activity of ORR of N-doped graphene stems from the electron-deficient carbon (Lewis base site) neighboring pyridinic nitrogen. The oxygen molecule is first adsorbed at these Lewis base sites created by pyridinic N, followed by protonation of the adsorbed O_2 (Figure 8). In the four-electron pathway, two protons cause the breakage of the O–OH bond and the formation of adsorbed OH, followed by the reaction of proton and OH species to form H_2O. The two-step two-electron pathway is also possible, where H_2O_2 is formed by the reaction of adsorbed OOH species and one proton before its reduction to H_2O.

Sulfur, boron, and phosphorous are also common dopants to enhance the ORR activity of graphene. S-doped graphene exhibited better ORR catalytic activity than the commercial Pt/C in alkaline media via breaking of electroneutrality of the graphitic planes.[109] A theoretical study showed that active catalytic sites locate at the zigzag edge or the neighboring carbon atoms of doped sulfur oxide atoms, which follow a four-electron transfer pathway.[110] B-doped graphene also showed similar electrocatalytic activity toward ORR as Pt-based catalysts, along with superior long-term stability and good CO tolerance to Pt catalysts.[111] The boron atoms with high local positive charges and the neighboring C atoms with high spin densities are the main active sites for ORR.[112] P-doped graphene (~0.92 V) exhibited a similar ORR onset potential as the commercial Pt/C (~0.95 V), as well as better selectivity and stability.[113] The excellent performance was ascribed to the activation of π-electrons in graphene by the phosphorous atoms.

Multi-doped graphene materials can achieve excellent ORR activity, such as N, P co-doped graphene,[54] B, N, and P tri-doped graphene,[114] N, F, and P tri-doped graphene,[115] and quaternary (B, N, P, and S) doped graphene.[52] Co-doping with two appropriate elements could lower the energy gap to increase the conductivity and chemical reactivity.[5] The redistribution of spin and charge densities induced by dual dopants increased the amounts of active sites for ORR reaction.[5] Co-doped and tri-doped graphene apparently exhibit higher efficiency for ORR than a single element doped one under the same conditions. However, it is difficult to control doping content, bonding formation, and distributional uniformity during co-doped graphene preparation processes.[14] The exact role of each dopant on the ORR performance and the underlying synergistic effect need extensive investigation.

4.2 | Graphene-based anodes

The large surface area, high electrical conductivity, and tunable anchoring sites of graphene-based materials can increase the dispersion of the noble metal and facilitate charge mobility in fuel oxidation. Great efforts have been made to develop efficient graphene-supported electrocatalysts for methanol oxidation reaction (MOR), ethanol oxidation reaction (EOR), and formic acid oxidation reaction (FAOR). Graphene-based materials are also promising as anode for microbial fuel cell (MFC) due to their high charge transport rate and biocompatibility.

4.2.1 | MOR electrocatalysts

DMFCs can generate electricity directly from methanol, a liquid fuel with a high volumetric energy density that is easy for transportation and storage, but its electrochemical reactivity is lower than hydrogen.[16] Moreover, the active sites of commonly used platinum-based catalysts are easily blocked by the reaction intermediates.[16] Graphene-based materials are promising for immobilizing Pt nanoparticles to enhance their activity and durability for MOR. For example, Yoo et al[116] reported higher efficiency of the Pt/rGO catalyst for MOR and 40 times slower CO adsorption rate than those of Pt/carbon black catalyst. The high-performance of Pt/rGO was attributed to the strong interaction between GNS and platinum atoms, leading to a decrease in Pt particle size and thus an increase in catalytic activity. The MOR current was further improved by ~3 times using N-doped rGO as support.[117] The amino and pyridinic groups on N-doped rGO can provide more anchoring sites for Pt nanoparticles and make their dispersion more uniform.[117,118] Apart from Pt-based catalysts, Pd- and Ni-based catalysts are also promising for catalyzing MOR in alkaline media due to their similar properties, lower cost, and higher CO tolerance.[119,120] The Pd/GNS displays higher MOR activity than Pd/carbon nanotubes and Pd/nanocarbon particles in 1 mol/L KOH due to its improved electrochemical active surface area (ECSA) of Pd nanoparticles on the graphene support.[119] The nonprecious Ni/rGO catalyst exhibited an ultrahigh mass activity of 1600 mA mg^{-1} and good anti-poisoning properties for MOR in 1 mol/L KOH, which was ascribed to the anchoring effects of rGO toward highly dispersed Ni nanoparticles.[120] Furthermore, graphene-based materials are suitable as supporting materials for bimetallic MOR catalysts due to their large specific surface area and electroconductivity, as well as flexible microstructure. Various highly efficient graphene-supported bimetallic MOR catalysts were reported recently, such as Pd@Ni/S doped graphene,[56] Pt-Pd nanoflowers/GO,[57] and Pt-Ni/porous rGO.[64]

The 3D graphene can accelerate the diffusion and mass transport of fuels and products. Owing to the hierarchical porous graphene framework, the 3D-structured graphene-supported Pt catalyst showed a more negative onset potential (0.17 V vs Ag/AgCl) and higher peak current density (443 mA mg^{-1} Pt) for MOR than commercial Pt/C catalyst.[121] Another Pt-Au alloy decorated 3D graphene prepared using aerosol spray drying exhibited about 6 times larger ECSA (325 m^2 mg^{-1} Pt) compared to Pt-Au/graphene (53 m^2 mg^{-1} Pt) and commercial Pt/carbon black (54 m^2 mg^{-1} Pt).[122] Recently, Qiu et al[123] synthesized 3D holey rGO hollow nanospheres sandwiched by interior and exterior Pt nanoparticles (Pt@holely r-GO@Pt hollow nanospheres) with SiO_2 nanosphere templates (Figure 9). The Pt@holely r-GO@Pt hollow nanospheres presented a 1.3-fold and 1.7-fold larger mass activity for MOR than those of Pt@r-GO@Pt hollow nanospheres and commercial Pt/C, which was attributed to the enhanced mechanical strength and mass diffusion, along with more exposed active sites. Huang and coworkers proposed a facile self-assembly strategy for the preparation of Pt nanoparticles coupled with 3D graphene cross-linked

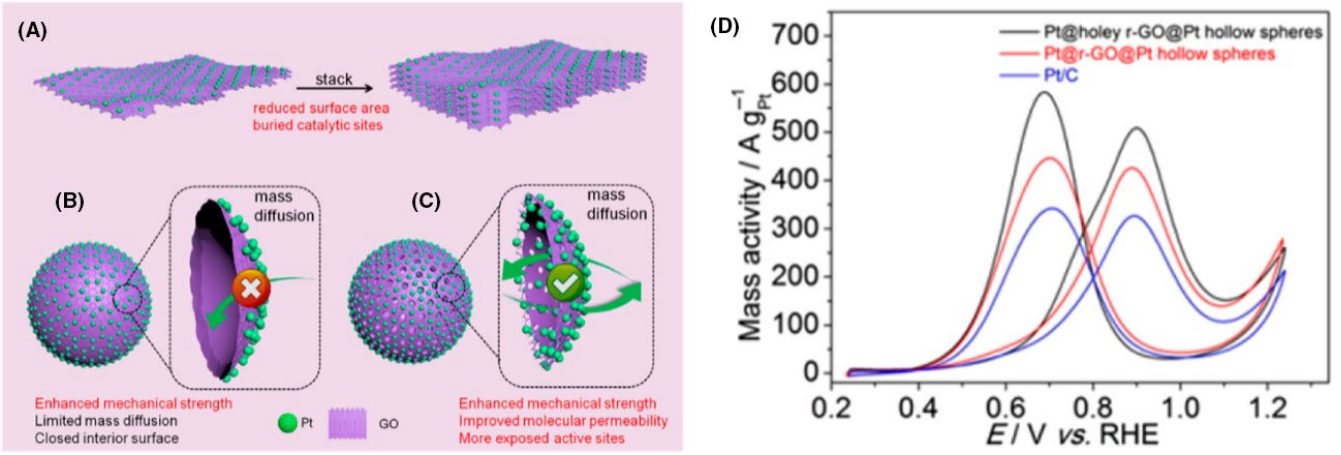

FIGURE 9 Schematic configurations of (A) 2D GO nanosheet-supported Pt nanoparticles, (B) 3D GO hollow nanosphere-supported Pt nanoparticles (Pt@r-GO@Pt hollow nanospheres), and (C) 3D holey GO hollow nanosphere sandwiched by both internal and external Pt nanoparticles (Pt@holely r-GO@Pt hollow nanospheres). (d) Pt mass-normalized cyclic voltammograms curves recorded in an N_2-saturated 0.5 mol/L H_2SO_4 + 0.5 mol/L CH_3OH solution with a sweep rate of 50 mV s^{-1}. Reprinted with permission from Ref.[123] Copyright 2018 American Chemical Society

hybrid architectures.[124-126] With large surface areas, high electrical conductivity, highly interconnected porous frameworks, and homogeneous Pt dispersion, these 3D graphene materials exhibited exceptional electrocatalytic performance for MOR. For example, the 3D Pt/RGO–$Ti_3C_2T_x$ architectures exhibited 3.7 times higher ECSA (90.1 m^2 g^{-1}) than that of Pt/C (24.6 m^2 g^{-1}), which was attributed to the strong electronic interactions of hybrid support and Pt nanoparticles.[126] The Pt/RGO–$Ti_3C_2T_x$ also showed higher electrocatalytic stability (~14.3% loss after 100 cyclic voltammetry cycles) than other state-of-the-art MOR catalysts.

4.2.2 | EOR electrocatalysts

Ethanol is a green energy source that can be produced from renewable agricultural feedstocks or biomass. Ethanol has higher mass energy density (8.01 kWh kg^{-1}) with less toxicity as compared to that (6.07 kWh kg^{-1}) of methanol.[17] Similar to MOR, noble metals are required to break the C–C bond in ethanol to complete oxidation and reduce the overpotential loss. Graphene-based materials are good supports to increase the dispersion of the noble metal and facilitate charge transfer. For example, Wang et al[127] prepared a hybrid electrode with an alternate assembly of two layers of Au nanoparticles and two layers of rGO sheets. The high electrochemical activity for EOR in alkaline medium was attributed to the oxidation removal of intermediates by highly conductive rGO. Huang et al[128] reported that the Pd/$Ni(OH)_2$/rGO catalyst exhibited a high peak current of 1500 mA mg^{-1} Pd and retained as 400 mA mg^{-1} after the chronoamperometric test of 20 000 seconds. The remaining oxygenated functionality on the rGO surface was thought to serve as nucleating sites for Pd nanoparticles, which benefits Pd dispersion. Similarly, the Pd-Au alloy/rGO catalyst showed 6.15-fold of mass activity for EOR in alkaline conditions than commercial Pd/C since rGO decreased the aggregation of nanoparticles.[129] These synergistic effects in the presence of graphene were also reported for Pt-Cu/GO,[60] Pt-Pd/rGO,[65] and Pd-Rh/GNS,[130] indicating the potential role of graphene as EOR catalyst support.

Modification of graphene with heteroatom and functional groups provides more anchor sites for metal nanoparticles, which largely promote EOR activity and durability.[131,132] Yang et al[131] prepared aniline-functionalized graphene by a diazo reaction to anchor Pd nanoparticles for EOR. The mass activity after the 7200 seconds test of the catalyst with aniline groups (43.1 mA mg^{-1}) was about 5 times higher than that (8.9 mA mg^{-1}) without aniline modification, which was attributed to the highly distribute Pd nanoparticles and the strong interaction between aniline groups and Pd. The 3D-structured graphene can also reduce the aggregation and deactivation of catalysts and enhance ethanol transport.[133,134] Yao et al[134] synthesized Pd encapsulated into hollow N-doped graphene microspheres by a spray-drying approach using GO and ZIF-8 as precursors, demonstrating a higher EOR activity (2490 mA mg^{-1}) than Pd/rGO (1232 mA mg^{-1}) in alkaline mediums. The hollow N-doped graphene microspheres not only benefited the immobilization of Pd nanoparticles but also facilitated the reactant diffusion.

4.2.3 | Other fuel oxidation reaction electrocatalysts

Apart from H_2, methanol, and ethanol, other fuels have been used for fuel cells, including formic acid, glycol, and

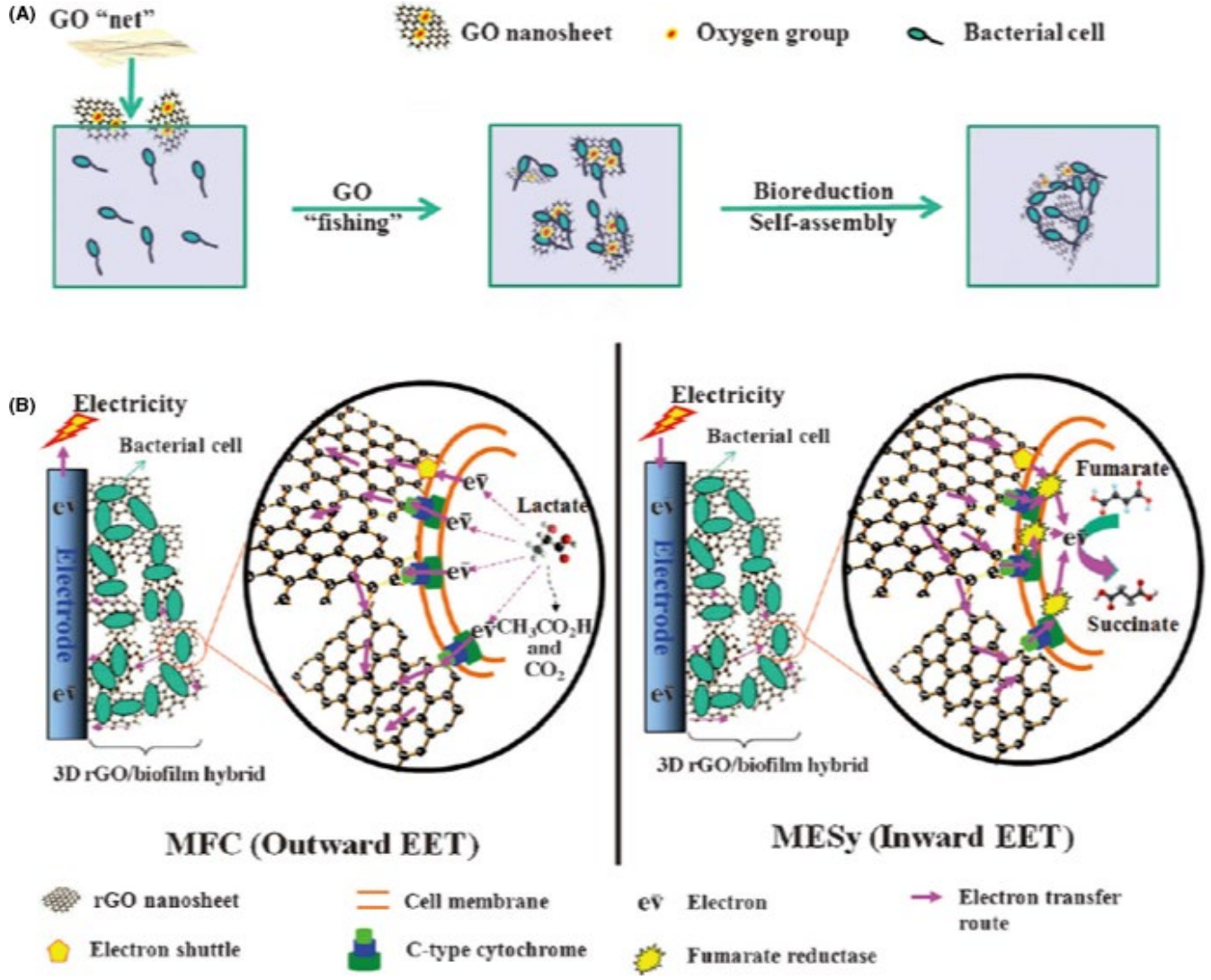

FIGURE 10 (A) The preparation process and (B) the proposed mechanism for extracellular electron transfer (EET) of rGO hybridized biofilm in an MFC. Reprinted with permission from Ref.[139] Copyright 2014 John Wiley and Sons

carbohydrazide.[135-138] Fan et al[135] reported Pd nanoflowers on phosphomolybdic acid-modified graphene for FAOR, demonstrating an 8-fold forward peak current density (1.02 A mg^{-1}) than that (0.13 A mg^{-1}) of Pd nanoparticles/graphene counterpart. The superior activity was attributed to the abundant defects of nanoflower shape, the strong CO oxidizing ability of phosphomolybdic acid, and the large interface area with strong binding between Pd, phosphomolybdic acid, and graphene. Another promising design strategy for FAOR is the use of F-doped graphene to support rhodium nanoparticles.[136] The stability of Rh/F-doped graphene was greatly improved, maintaining 65% of activity after 100 cycles compared to that (40%) of Pt/C catalyst. Feng et al[137] supported core-shell Au@AuPd on rGO, and observed its superior glycol oxidation performance than Pd/C catalyst due to the synergetic effects of core-shell nanostructures and rGO support. Hu and coworkers developed a metal-free 3D graphene anode for carbohydrazide oxidation reaction, which showed an activity enhancement of 2 times compared to 2D graphene due to the larger surface area and higher electronic conductivity.[138] An anion exchange membrane fuel cell (AEMFC) coupled with 3D graphene anode and N-doped carbon nanotubes cathode generated a peak power density of 24.9 mW cm^{-2}.

4.2.4 | MFC anodes

MFCs are sustainable energy generation devices that convert biomass or organic waste to electricity via the metabolism of microorganisms. Graphene-based materials have a large surface area, good conductivity, and biocompatibility, which can reduce the internal resistance of the anode, act as a mediator to accelerate the electron transfer between bacteria and anode, and promote bacterial growth of MFCs.[2] For example, Yong et al[139] hybridized highly conductive rGO with bacteria

on carbon cloth to fabricate MFC anode, showing a 25-fold increase in the oxidation current (0.52 mA cm^{-2}) and a 74-fold increase in the reduction current (0.82 mA cm^{-2}) when compared with anodes without rGO. The extraordinary performance of the MFC was attributed to the enhanced extracellular electron transfer capability by rGO via multiplexed conductive pathways (Figure 10). To further improve the bacterial adhesion capability and the interactions between bacteria and the electrode surface of MFC anode, Luo et al[140] prepared crumpled graphene via a capillary compression approach. The rough surface of crumpled rGO benefited biofilm formation and thus largely enhanced the MFC performance, delivering 31% and 116% higher maximum power density than that with flat rGO and activated carbon, respectively.

Recent works have demonstrated the advantages of 3D graphene applied in MFCs, not only extending the active area for bacteria attachment and mediator reduction but also reducing the diffusion resistance via hierarchical open-porous structure.[141-145] Ren et al[141] developed a 3D macroporous graphene scaffold anode, exhibiting a maximum power density of 11 220 W m^{-3} due to its hierarchical porous structure and low internal resistance. Li et al[145] found that increasing the hydrophilicity of 3D graphene aerogel by GO modification can notably improve the biofilm density on the anode and thus enhance the MFC performance. Further doping nitrogen into graphene, the MFC with 3D N-doped graphene aerogel anode delivered a stable current in at least 5 days.[142] Song et al[144] incorporated a core/satellite structured Fe_3O_4/Au nanocomposite on 3D macroporous graphene foam to improve the anode/bacteria interaction and bacterial penetration, achieving a 71-fold higher power density (2980 mW m^{-2}) than that of graphite rod anode (41 mW m^{-2}).

4.3 | Graphene-based membranes

The electrolytes in a fuel cell need high ionic conductivity, electrical insulation, and low permeability for reactants. The most commonly used polymeric membrane in PEMFCs is Nafion, exhibiting high proton conductivity and chemical stability.[1] However, its performance is limited by hydrated conditions, operating temperature, and fuel crossover issues.[6] Graphene-based materials have been explored as fillers to enhance the ionic conductivity and reduce the gas permeability of polymer membranes, or even as proton-conducting electrolytes for fuel cells.

4.3.1 | Graphene and GO membrane

Hu et al[7] firstly proved that thermal protons could transport through monolayer graphene with activation energy of about 0.78 eV under ambient conditions (Figure 11A). Its proton conductivity can meet fuel cell requirements (>1 S cm^{-2}) when the temperature is higher than 110°C, and reach as high as 10^3 S cm^{-2} at temperatures above 250°C. The proton conductivity of monolayer graphene can be further improved by decorated with Pt (Figure 11B).

Although monolayer graphene presents high proton conductivity at a moderately high temperature, its high electrical conductivity impedes directly using it as a membrane material for fuel cells. Instead, the properties of electrical insulator, gas impermeability, and hydrophilicity of GO make it as a promising electrolyte in fuel cells. Tateishi et al[73] first reported the performance of a fuel cell using a pure GO paper membrane. The MEA with a configuration of Pt | GO | Pt can output a maximum power density of ~13 mW cm^{-2} at a relative humidity of <20% and room temperature. Gao et al[75] investigated the proton transport through the ozonated GO membrane and its fuel cell performance. The proton conductivity of the ozonated GO membrane is 50% higher than that of the GO membrane, which was ascribed to the enhanced proton hopping via higher content of oxygenated functional groups. Furthermore, sulfonic acid functionalized GO exhibited 14 times higher proton conductivity (58 mS cm^{-1} at 55°C) than unmodified GO due to enhancing the mobility of oxonium ions combined with water molecules.[146]

4.3.2 | Graphene-modified polymer membranes

Graphene-based materials are commonly used to decorate on polymer membranes to enhance their ionic conductivity and gas impermeability. The composite membranes exhibit higher ionic conductivity, lower fuel gas permeability, higher mechanical strength, and higher chemical stability than traditional polymer membranes, thus improving fuel cell performance and durability.

The presence of intrinsic defects at different dimensions and cracks and protonated carboxylic groups on GO surface would enhance their proton conductivity.[68,77] Furthermore, the homogeneously distributed GO sheets in the polymer matrix can increase its ionic transport via well-connected 3D ionic channels.[67,147] For example, by incorporating 0.5 wt% ionic liquid polymer-modified graphene sheets, the ionic conductivity (7.5×10^{-3} S cm^{-1} at 160°C) of sulfonated polyimide membrane was improved by about 2.6 times.[147] However, a higher proportion of graphene sheets would overlap with each other, blocking the ionic transfer route and formation of an electrical conducting network.[67] Aragaw et al[148] reported the proton conductivity of an rGO/Nafion is 30 times higher than unmodified Nafion, which was ascribed to the alignment change of the proton channels parallel to the membrane surface. Jia et al[69] reported that a slightly reduced GO/Nafion 117 composite membrane could form a long-range order of 3D

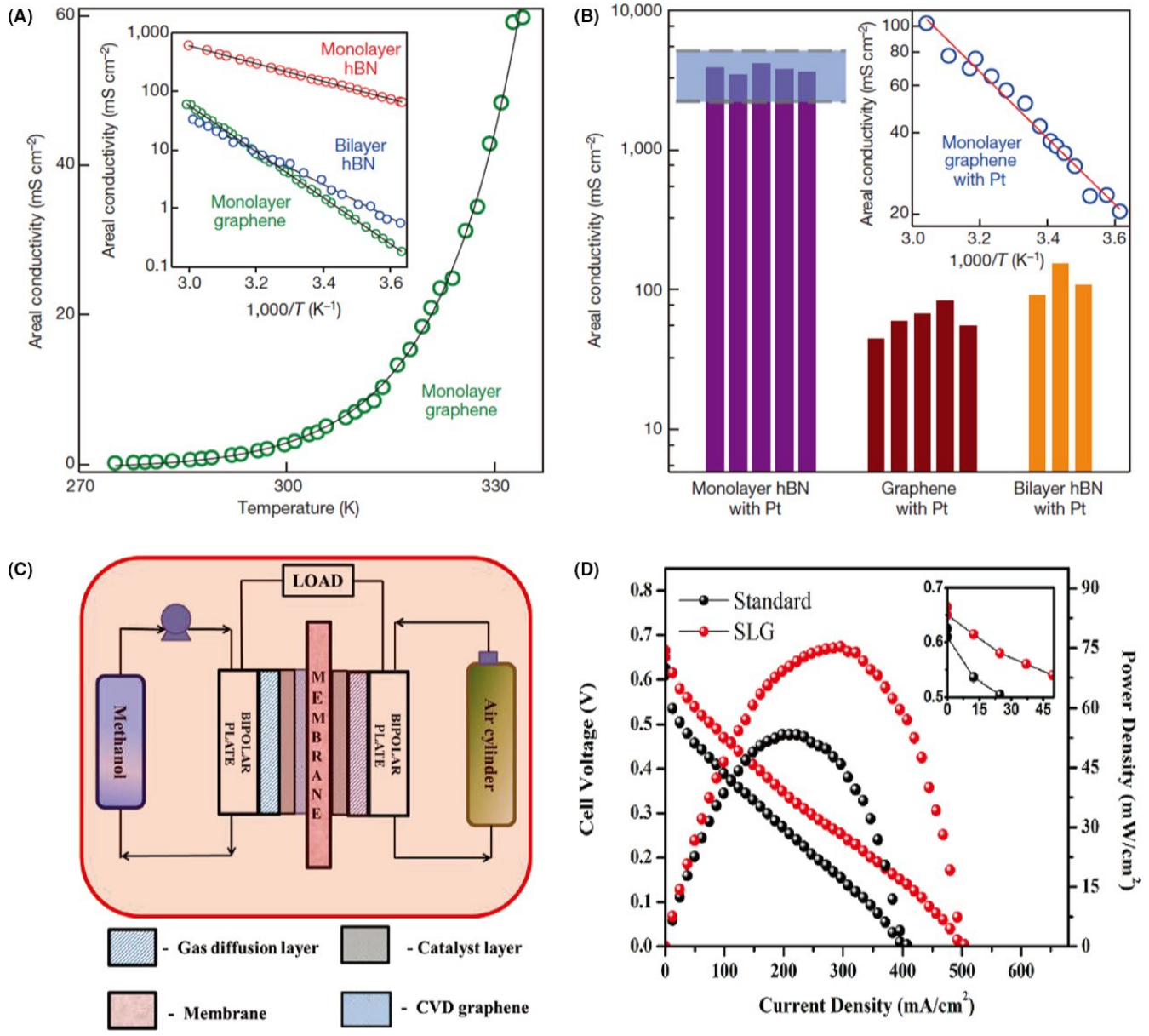

FIGURE 11 (A) Temperature dependences of proton conductivity for graphene and hexagonal boron nitride (hBN). (B) Proton conductivity of graphene and hBN decorated with Pt. Insert is the Arrhenius-type behavior for these membranes. Reprinted with permission from Ref.[7] Copyright 2014 Springer Nature. (C) DMFC experimental setup and MEA configuration. (D) Polarization curve comparison for a standard MEA and an MEA with single-layer graphene (SLG) at 70°C, 1 mol/L methanol, 1 L min^{-1} of air. Insert is the magnified view of open-circuit voltages of each MEA. Reprinted with permission from Ref.[76] Copyright 2016 John Wiley and Sons

ionic nanochannels by self-assembly, exhibiting near 4-fold enhancement in proton conductivity. Graphene is flexible for functionalization with proton-conducting groups like sulfonic acid to further facilitate proton transport. For instance, Qiu et al[70] showed that the sulfonated rGO/SPEEK exhibited threefold higher proton conduction than pristine SPEEK at low relative humidity due to the higher water retention capability of sulfonic acid groups. Another sulfonated holey GO modified SPEEK (SPEEK/SHGO) was synthesized by etching sulfonated GO with concentrated HNO_3 under ultrasonication.[71] The presence of the holes in the sulfonated holey GO provided an additional channel for proton transport, further increasing the proton conductivity to 135.9 mS cm^{-1} at 65°C, which is larger than that (91.6 mS cm^{-1} at 65°C) of sulfonated GO/SPEEK. Graphene can also increase bicarbonate conductivity of QPSU in AFCs.[72] The quaternized graphene/QPSU composite membrane showed 4 times higher bicarbonate conductivity (18.73 mS cm^{-1} at 80°C) than pristine QPSU due to the continuous hydrophilic channels of the quaternary ammonium ion clusters and their water-absorbing ability.

A critical drawback of the Nafion membrane is fuel crossover, especially for methanol. Graphene-based materials can act as a barrier layer to impede fuel gas permeation without

sacrificing the proton conductivity, leading to an increase in fuel utilization efficiency and overall fuel cell performance. Holmes et al[76] decorated pristine monolayer graphene on the anode side of MEA of a DMFC (Figure 11C) and observed that methanol crossover decreased with increasing graphene coverage. When operating temperature is higher than 60°C, the proton conductivity of graphene is higher than the Nafion membrane, thus eliminating the increments on the proton resistance. As a result, the DMFC with graphene showed a 45% improvement in power density than the DMFC without graphene (Figure 11D). Yan et al[77] developed a composite membrane with monolayer graphene sandwiched by two layers of Nafion 212. The methanol permeability significantly decreased from 1.40×10^{-6} to 0.44×10^{-6} cm^2 s^{-1} with graphene incorporation, achieving a high peak power density of 23 mW cm^{-2} at highly concentrated 10 mol/L methanol. Moreover, a sulfonated GO/Nafion membranes showed good methanol barrier properties due to its steric hindrance effect and the shrinkage of ionic clusters.[149] The methanol permeability of a slightly reduced GO/Nafion 117 composite membrane is two-magnitude lower than that of Nafion 117.[69]

The mechanical properties of polymer membranes can also be significantly improved by graphene. It was revealed that the tensile strength of GO/Nafion composite membrane increased with GO content, reaching about 8-fold improvement with 4.5 wt.% GO content.[68] The quaternized graphene/QPSU with 0.5 wt% loading exhibited a nearly 3-fold increase in Young's modulus (5240 MPa) and tensile strength (205 MPa).[72] The PVA/graphene with 1.4 wt.% graphene loading demonstrated a 73% enhancement in the tensile strength due to the enhancement in the adhesion of the nanofiller and matrix.[67] Moreover, graphene-based fillers could also enhance the long-term stability of membranes. For example, the cell with SPEEK/SHGO membrane maintained ~88.6% of the initial output voltage after 60 hours operation at the current density of 50 mA cm^{-2}, which is significantly higher than that of pristine SPEEK (61.7%).[71] The higher durability was attributed to the compatibilizing effect of the SHGO on the SPEEK via both hydrophobic and hydrophilic interactions between them. Another rGO/Nafion membrane presented only a slight decrease of proton conductivity (from 0.58 to 0.52 S cm^{-1}) after 720 minutes of immersion in methanol.[69]

4.4 | Graphene-based bipolar plates

Bipolar plates are used for current collection, gas and heat distribution, and mechanical support in fuel cells. The idea bipolar plates should have high electrical and thermal conductivity, low interfacial contact resistance, low permeability to gases, high corrosion resistance, high mechanical strength, lightweight, and low cost.[8] Graphite is the most preferred material for bipolar plates in PEMFCs due to its high corrosion resistance and considerable conductivity (10^3 S cm^{-1}), but its mechanical strength is poor and its fabrication cost is relatively high.[1,8] Metallic bipolar plates have high electrical conductivity and high mechanical strength, but their corrosion-resistant in the acidic environment is not sufficient.[1,8] These disadvantages have promoted the development of alternative bipolar plates with graphene modification.

Graphene with anti-corrosive nature has been used as a protective layer for metallic bipolar plates. Ren et al[150] reported a graphene-coated copper showed 3 times higher charge transfer resistance than uncoated copper in 720 hours of immersion of 0.5 mol/L H_2SO_4, demonstrating the high corrosion resistance of graphene-coated copper plates. Furthermore, a Cu/GO composite was coated on mild steel, showing a corrosion current of 10.03 μA cm^{-2} in 3.5 wt.% NaCl, which is about 30 times lower than uncoated mild steel.[151] This was attributed to the formation of enhanced passive film by {220} texture of Cu. Sim et al[152] coated multilayer graphene on Ni foam by a dip coating and rapid thermal annealing (RTA) with PMMA as carbon precursors (Figure 12A). The graphene/Ni foam bipolar plates showed two orders of magnitude lower corrosion rate than uncoated one (Figure 12B) and the embedded PEMFC demonstrated a peak power density of ~967 mW cm^{-2}, which meet the US Department of Energy (DOE) 2020 target (Figure 12C). Another benefit provided by the graphene/Ni foam is a more uniform distribution of local current and gas.

Graphene-based materials can also be used as fillers to develop highly conductive polymeric bipolar plates. Jiang et al[153] reported that an exfoliated graphene nanoplatelets/polyphenylene sulfide composite exhibited higher flexural modulus and low gas permeability, but its electrical conductivity (1.7 S cm^{-1}) was not sufficient. The addition of 20 wt.% carbon black enhanced its electrical conductivity to 114 S cm^{-1}. Plengudomkit et al[154] prepared a highly filled graphene/polybenzoxazine composites with 60 wt.% graphene content, exhibiting high flexural modulus (18 GPa), flexural strength (42 MPa), thermal conductivity (8.0 W/mK), electrical conductivity (357 S cm^{-1}), and low water absorption (0.06% at 24 hours immersion). Jiang et al[155] synthesized a GO/polypyrrole composite, followed by coating on 304 stainless steel using a in situ electrodeposition method. The presence of GO in the composite bipolar plates enhanced the interfacial adhesion between metal and polymer and prevented the corrosive species penetration.

However, challenges still remain for the use of graphene-based materials in bipolar plates. It was found that graphene showed no improvement in corrosion resistance at high temperature (>60°C) or for stainless steel plates without Ni coating or for Al plates, possibly due to the galvanic corrosion mechanism or the reaction between ions and defects/grain boundaries in graphene.[156,157] The relatively low electrical

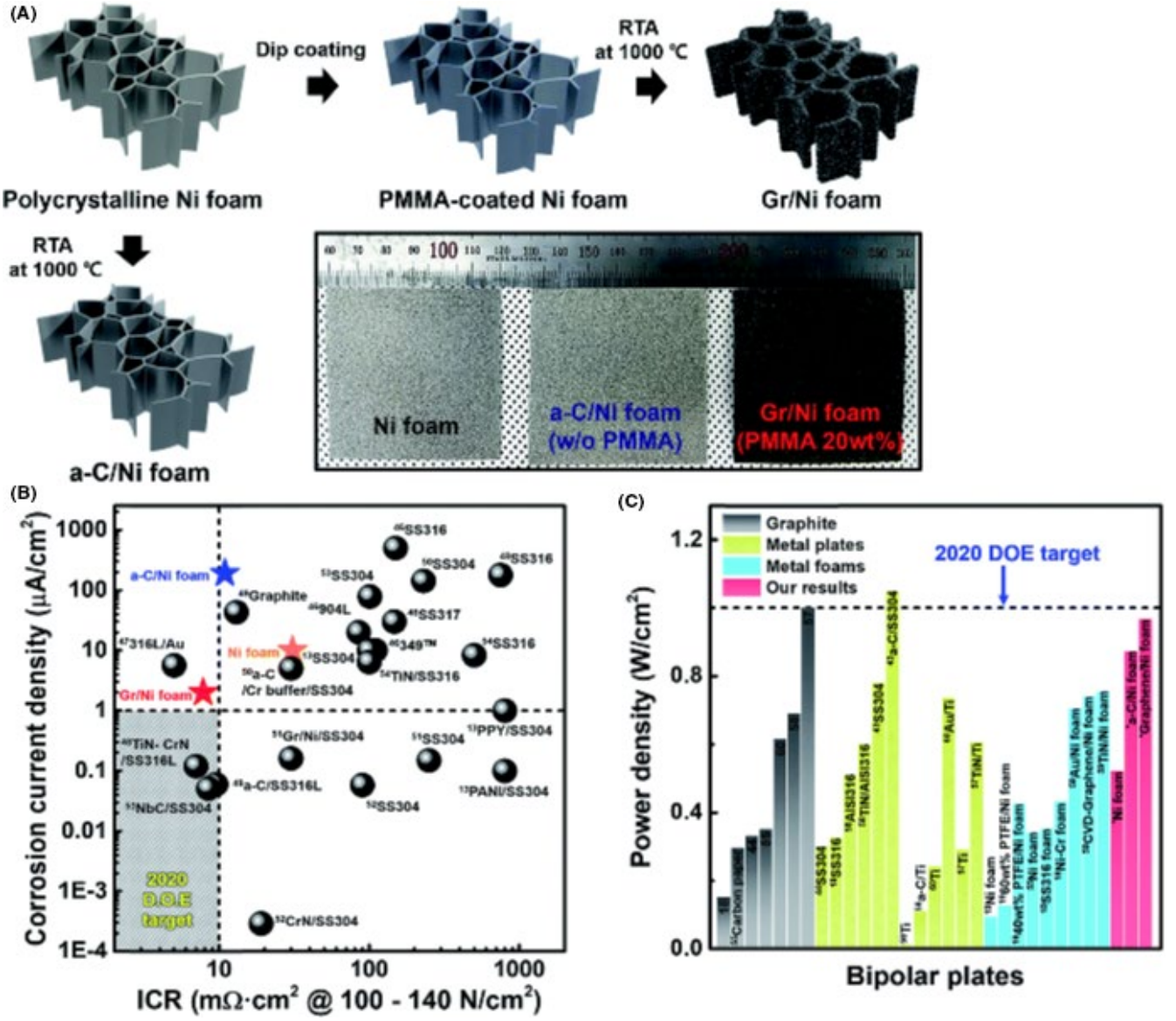

FIGURE 12 (A) Schematic of the synthesis of graphene/Ni foam. (B) Comparison of corrosion current density and interfacial contact resistance (ICR) at a pressure of 100-140 N/cm^2 of various reported bipolar plates. The gray area is the 2020 DOE target. (C) Power densities of PEMFC with graphene/Ni foam and other reported bipolar plates. The dashed line is the 2020 DOE target. Reprinted with permission from Ref.[152] Copyright 2018 Royal Society of Chemistry

conductivity of GO or rGO coatings may increase interfacial contact resistance. Moreover, adhesion of hydrophobic graphene on metallic plates without adding any binder is quite challenging.[8] The addition of binder would inevitably increase interfacial contact resistance and cost. Another challenge is to develop gas flow channels in the graphene structure without damaging its electrical and corrosion resistance properties.

5 | CONCLUSION AND OUTLOOK

This review summarized the progress associated with applications of graphene-based materials in fuel cells. Comparable to the commercial Pt/C catalyst, metal-free heteroatom-doped graphene shows high electroactivity for ORR. Doped graphene, GO, and rGO provide many anchoring sites for active metal particles, making them dispersion uniformly. The high surface area and electrical conductivity of graphene-supported catalysts favor various electrochemical reactions, such as ORR, MOR, EOR, and FAOR. The strong metal-graphene interaction leads to enhanced long-term stability. The novel 3D-structured graphene electrodes were recently developed, aiming at enhancing active sites and reducing diffusion resistance. Graphene and GO also exhibited high proton conductivity and low fuel permeation, enabling them act as alternative electrolyte materials or incorporate with polymer

membranes. Moreover, highly conductive and chemical stable graphene can protect metallic bipolar plates from corrosion. However, there are also some challenges that require further studies.

1. The underlying mechanism in the catalytic activity of heteroatom-doped graphene still remains blurred. Various types of dopants, functional groups, defects, and vacancies of graphene may act as catalytic active sites, but their features aimed to promote a given reaction should be explored in depth. Systematic and reliable characterization techniques and theoretical studies are required to identify the active sites and the corresponding electrocatalytic mechanisms. Controlling the graphene microstructure by selective passivation of the possible active sites is an efficient route to gain insights on active sites. Furthermore, the effects of the remaining impurities, especially trace metals in graphene induced during the fabrication process on the catalytic activity should be paid sufficient attention. Rigorous elemental analysis should be provided for so-called "metal-free" heteroatom-doped graphene. Preparing the metal-free graphene-based electrocatalysts via transition metal-free synthesis routes could eliminate this issue.
2. The proton conductivity of single-layer graphene and GO is not sufficient for fuel cell application. When using graphene-based materials as fillers in polymer membranes, there is a trade-off between barrier properties and proton conductivities. GO and functionalized graphene would block the continuity of proton conductive channels in the polymer membrane, thus the amount of loading should be carefully optimized. More efforts are necessary to evaluate the types of functional groups, architectures, compatibility with polymers of graphene-based fillers, and their relation to proton conductivity, impermeability, and fuel cell performance.
3. For most graphene-based electrocatalysts, their performances were only evaluated in the half-cell test, which cannot accurately represent their activities and durability under practical operating conditions. A possible solution to the issue would be to utilize the standard MEA systems for their performance assessment. Furthermore, the conductivity and permeability of graphene-based membranes and the corrosion resistance of graphene-modified bipolar plates should be evaluated under practical fuel cell environments rather than simple simulating conditions.
4. Stability is one of the main issues hampering the real commercialization of fuel cells with graphene-based materials. Although numerous graphene-based electrocatalysts demonstrated higher durability, better tolerance to methanol crossover and CO poisoning compared with commercial Pt/C, the reported preserving lifetimes of graphene-based fuel cells (in the range of a few hours to several weeks) are far away from the lifetime (in year scale) that is desirable for commercial applications. Most of the practical PEMFCs exploit acidic electrolytes to eliminate the effect of carbon dioxide, leading to the demetallation of graphene-supported metal catalyst and subsequent degradation during long-term operation. Metal-free doped-graphene catalysts are promising candidates, but rare cases are effective for ORR in acidic media to date. The defect-free graphene is highly stable and mechanically robust. However, defects, heteroatoms, and functional groups are always required to be introduced into graphene basal planes to obtain sufficient activity for fuel cell applications, which inevitably reduces their chemical and mechanical stability. Precise control of active sites and the graphitization degree of graphene-based materials is critical for achieving optimal performance.
5. Cost is another factor that influences manufacturing graphene-based materials for real fuel cell systems. Metal-free, PGM-free, or low-PGM graphene-based electrocatalysts showed great promise for replacing high-cost Pt/C catalysts. The larger surface area and higher mass activity further reduce the system costs by lowering the catalyst loading. However, the costs of synthesis, storage, and processing of graphene-based materials themselves should be taken into consideration. The graphene-modified membranes and bipolar plates also add an extra cost to the fuel cells. Transforming a lab-scale process to large-scale (up to tons scale) production is an efficient way to reduce the synthesis cost of the graphene-based materials. Roll-to-roll process, on-site polymerization, flash Joule heating method, and alkaline metal technologies are promising for scalable manufacturing of high-quality 2D and 3D graphene.[30,158] With the rapid commercialization of graphene, there is a steady trend of production increase and price decrease. For example, the price of graphene nanoplatelets decreased by 10-fold (from US\$250 kg^{-1} to US\$20 kg^{-1}) within 4 years.[158] However, the synthesis of graphene-based catalysts or membranes is available only in laboratories at present. Challenges remain to achieve economic viability for large-scale fabrication and application of graphene-based materials in fuel cell technologies.
6. Graphene-based materials have been only applied in low-temperature polymer membrane-based fuel cells (PEMFCs, AFCs, DMFCs, MFCs, etc). Excellent thermal stability of graphene can allow ones to expect its promising achievement in high-temperature MCFCs or SOFCs. Recently, graphene nanoplatelets or rGO were incorporated into yttria-stabilized zirconia (YSZ) as alternative interconnectors in SOFC, demonstrating the improved thermal conductivity, cracking resistance, and ionic conductivity.[159] This finding would stimulate further R&D efforts in the application of graphene-based materials for high-temperature fuel cells.

ACKNOWLEDGMENTS

This work was partially supported by US National Science Foundation (CMMI-1661699). The authors also thank Charles and Carroll McArthur for their great support.

CONFLICT OF INTEREST

There are no conflicts to declare.

ORCID

Yun Hang Hu https://orcid.org/0000-0002-5358-8667

REFERENCES

1. Steele BCH, Heinzel A. Materials for fuel-cell technologies. *Nature*. 2001;414(6861):345-352.
2. Li S, Cheng C, Thomas A. Carbon-based microbial-fuel-cell electrodes: from conductive supports to active catalysts. *Adv Mater*. 2017;29(8):1602547.
3. Zhou X, Qiao J, Yang L, Zhang J. A review of graphene-based nanostructural materials for both catalyst supports and metal-free catalysts in PEM fuel cell oxygen reduction reactions. *Adv Energy Mater*. 2014;4(8):1301523.
4. Yang L, Shui J, Du L, et al. Carbon-based metal-free ORR electrocatalysts for fuel cells: past, present, and future. *Adv Mater*. 2019;31(13):1804799.
5. Shao Y, Jiang Z, Zhang Q, Guan J. Progress in nonmetal-doped graphene electrocatalysts for the oxygen reduction reaction. *Chemsuschem*. 2019;12(10):2133-2146.
6. Perez-Page M, Sahoo M, Holmes SM. Single layer 2D crystals for electrochemical applications of ion exchange membranes and hydrogen evolution catalysts. *Adv Mater Interfaces*. 2019;6(7):1801838.
7. Hu S, Lozada-Hidalgo M, Wang FC, et al. Proton transport through one-atom-thick crystals. *Nature*. 2014;516(7530):227-230.
8. Singh RS, Gautam A, Rai V. Graphene-based bipolar plates for polymer electrolyte membrane fuel cells. *Front Mater Sci*. 2019;13(3):217-241.
9. Zhu Y, Murali S, Cai W, et al. Graphene and graphene oxide: synthesis, properties, and applications. *Adv Mater*. 2010;22(35):3906-3924.
10. Ambrosi A, Chua CK, Bonanni A, Pumera M. Electrochemistry of graphene and related materials. *Chem Rev*. 2014;114(14):7150-7188.
11. Navalon S, Dhakshinamoorthy A, Alvaro M, Garcia H. Carbocatalysis by graphene-based materials. *Chem Rev*. 2014;114(12):6179-6212.
12. Ambrosi A, Chua CK, Latiff NM, et al. Graphene and its electrochemistry - an update. *Chem Soc Rev*. 2016;45(9):2458-2493.
13. Chen D, Feng H, Li J. Graphene oxide: preparation, functionalization, and electrochemical applications. *Chem Rev*. 2012;112(11):6027-6053.
14. Kong XK, Chen CL, Chen QW. Doped graphene for metal-free catalysis. *Chem Soc Rev*. 2014;43(8):2841-2857.
15. Huang H, Yan M, Yang C, et al. Graphene nanoarchitectonics: recent advances in graphene-based electrocatalysts for hydrogen evolution reaction. *Adv Mater*. 2019;31(48):e1903415.
16. Siwal SS, Thakur S, Zhang QB, Thakur VK. Electrocatalysts for electrooxidation of direct alcohol fuel cell: chemistry and applications. *Mater Today Chem*. 2019;14:100182.
17. Bai J, Liu D, Yang J, Chen Y. Nanocatalysts for electrocatalytic oxidation of ethanol. *Chemsuschem*. 2019;12(10):2117-2132.
18. Liu M, Zhang R, Chen W. Graphene-supported nanoelectrocatalysts for fuel cells: synthesis, properties, and applications. *Chem Rev*. 2014;114(10):5117-5160.
19. Yadav R, Subhash A, Chemmenchery N, Kandasubramanian B. Graphene and graphene oxide for fuel cell technology. *Ind Eng Chem Res*. 2018;57(29):9333-9350.
20. Shaari N, Kamarudin SK. Graphene in electrocatalyst and proton conductiong membrane in fuel cell applications: an overview. *Renew Sust Energ Rev*. 2017;69:862-870.
21. Iqbal MZ, Rehman A-U, Siddique S. Prospects and challenges of graphene based fuel cells. *J Energy Chem*. 2019;39:217-234.
22. Novoselov KS, Geim AK, Morozov SV, et al. Electric field effect in atomically thin carbon films. *Science*. 2004;306(5696):666-669.
23. Sun Z, Hu YH. How magical is magic-angle graphene? *Matter*. 2020;2(5):1106-1114.
24. Wang X-Y, Narita A, Müllen K. Precision synthesis versus bulk-scale fabrication of graphenes. *Nat Rev Chem*. 2017;2(1):1-10.
25. Gao W, Singh N, Song L, et al. Direct laser writing of micro-supercapacitors on hydrated graphite oxide films. *Nat Nanotechnol*. 2011;6(8):496-500.
26. Poh HL, Šimek P, Sofer Z, Tomandl I, Pumera M. Boron and nitrogen doping of graphene via thermal exfoliation of graphite oxide in a BF_3 or NH_3 atmosphere: contrasting properties. *J Mater Chem A*. 2013;1(42):13146-13153.
27. Seredych M, Bandosz TJ. S-doped micro/mesoporous carbon–graphene composites as efficient supercapacitors in alkaline media. *J Mater Chem A*. 2013;1(38):11717-11727.
28. Fei Y, Fang S, Hu YH. Synthesis, properties and potential applications of hydrogenated graphene. *Chem Eng J*. 2020;397:125408.
29. Eng AYS, Sofer Z, Šimek P, Kosina J, Pumera M. Highly hydrogenated graphene through microwave exfoliation of graphite oxide in hydrogen plasma: towards electrochemical applications. *Chem Eur J*. 2013;19(46):15583-15592.
30. Sun Z, Fang S, Hu YH. 3D graphene materials: from understanding to design and synthesis control. *Chem Rev*. 2020;120(18):10336-10453.
31. Sun H, Zhu J, Baumann D, et al. Hierarchical 3D electrodes for electrochemical energy storage. *Nat Rev Mater*. 2018;4(1):45-60.
32. Wu ZS, Yang S, Sun Y, Parvez K, Feng X, Mullen K. 3D nitrogen-doped graphene aerogel-supported Fe_3O_4 nanoparticles as efficient electrocatalysts for the oxygen reduction reaction. *J Am Chem Soc*. 2012;134(22):9082-9085.
33. Chang L, Hu YH. Breakthroughs in designing commercial-level mass-loading graphene electrodes for electrochemical double-layer capacitors. *Matter*. 2019;1(3):596-620.
34. Li G, Huang B, Pan Z, Su X, Shao Z, An L. Advances in three-dimensional graphene-based materials: configurations, preparation and application in secondary metal (Li, Na, K, Mg, Al)-ion batteries. *Energy Environ Sci*. 2019;12(7):2030-2053.
35. Wang H, Hu YH. Graphene as a counter electrode material for dye-sensitized solar cells. *Energy Environ Sci*. 2012;5(8):8182.
36. El-Kady MF, Strong V, Dubin S, Kaner RB. Laser scribing of high-performance and flexible graphene-based electrochemical capacitors. *Science*. 2012;335(6074):1326-1330.
37. Xu Z, Sun H, Zhao X, Gao C. Ultrastrong fibers assembled from giant graphene oxide sheets. *Adv Mater*. 2013;25(2):188-193.
38. Chang L, Stacchiola DJ, Hu YH. An ideal electrode material, 3D surface-microporous graphene for supercapacitors with ultrahigh areal capacitance. *ACS Appl Mater Interfaces*. 2017;9(29):24655-24661.

39. Matsumoto M, Saito Y, Park C, Fukushima T, Aida T. Ultrahigh-throughput exfoliation of graphite into pristine 'single-layer' graphene using microwaves and molecularly engineered ionic liquids. *Nat Chem*. 2015;7(9):730-736.
40. Xu Y, Sheng K, Li C, Shi G. Self-assembled graphene hydrogel via a one-step hydrothermal process. *ACS Nano*. 2010;4(7):4324-4330.
41. Voiry D, Yang J, Kupferberg J, et al. High-quality graphene via microwave reduction of solution-exfoliated graphene oxide. *Science*. 2016;353(6306):1413-1416.
42. Fang S, Lin Y, Hu YH. Recent advances in green, safe, and fast production of graphene oxide via electrochemical approaches. *ACS Sustain Chem Eng*. 2019;7(15):12671-12681.
43. Li X, Cai W, An J, et al. Large-area synthesis of high-quality and uniform graphene films on copper foils. *Science*. 2009;324(5932):1312-1314.
44. Chen Z, Ren W, Gao L, Liu B, Pei S, Cheng HM. Three-dimensional flexible and conductive interconnected graphene networks grown by chemical vapour deposition. *Nat Mater*. 2011;10(6):424-428.
45. Wang H, Sun K, Tao F, Stacchiola DJ, Hu YH. 3D honeycomb-like structured graphene and its high efficiency as a counter-electrode catalyst for dye-sensitized solar cells. *Angew Chem Int Ed Engl*. 2013;52(35):9210-9214.
46. Chang L, Sun K, Hu YH. New chemistry for new material: highly dense mesoporous carbon electrode for supercapacitors with high areal capacitance. *ACS Appl Mater Interfaces*. 2018;10(39):33162-33169.
47. Wei W, Sun K, Hu YH. Direct conversion of CO_2 to 3D graphene and its excellent performance for dye-sensitized solar cells with 10% efficiency. *J Mater Chem A*. 2016;4(31):12054-12057.
48. Wei W, Chang L, Sun K, et al. The bright future for electrode materials of energy devices: highly conductive porous Na-embedded carbon. *Nano Lett*. 2016;16(12):8029-8033.
49. Luong DX, Bets KV, Algozeeb WA, et al. Gram-scale bottom-up flash graphene synthesis. *Nature*. 2020;577(7792):647-651.
50. Sun Z, Hu YH. Ultrafast, low-cost, and mass production of high-quality graphene. *Angew Chem Int Ed*. 2020;59(24):9232-9234.
51. Qu L, Liu Y, Baek J-B, Dai L. Nitrogen-doped graphene as efficient metal-free electrocatalyst for oxygen reduction in fuel cells. *ACS Nano*. 2010;4(3):1321-1326.
52. Molina-García MA, Rees NV. "Metal-free" electrocatalysis: quaternary-doped graphene and the alkaline oxygen reduction reaction. *Appl Cata A*. 2018;553:107-116.
53. Xia W, Tang J, Li J, et al. Defect-rich graphene nanomesh produced by thermal exfoliation of metal-organic frameworks for the oxygen reduction reaction. *Angew Chem Int Ed Engl*. 2019;58(38):13354-13359.
54. Chai G-L, Qiu K, Qiao M, Titirici M-M, Shang C, Guo Z. Active sites engineering leads to exceptional ORR and OER bifunctionality in P, N Co-doped graphene frameworks. *Energy Environ Sci*. 2017;10(5):1186-1195.
55. Jeon IY, Zhang S, Zhang L, et al. Edge-selectively sulfurized graphene nanoplatelets as efficient metal-free electrocatalysts for oxygen reduction reaction: the electron spin effect. *Adv Mater*. 2013;25(42):6138-6145.
56. Perivoliotis DK, Sato Y, Suenaga K, Tagmatarchis N. Sulfur-doped graphene-supported nickel-core palladium-shell nanoparticles as efficient oxygen reduction and methanol oxidation electrocatalyst. *ACS Appl Energy Mater*. 2018;1(8):3869-3880.
57. Xu L, Cui Q, Zhang H, et al. Ultra-clean PtPd nanoflowers loaded on GO supports with enhanced low-temperature electrocatalytic activity for fuel cells in harsh environment. *Appl Surf Sci*. 2020;511:145603.
58. Cheng Y, He S, Lu S, et al. Iron single atoms on graphene as non-precious metal catalysts for high-temperature polymer electrolyte membrane fuel cells. *Adv Sci*. 2019;6(10):1802066.
59. Qiu X, Yan X, Pang H, et al. Isolated Fe single atomic sites anchored on highly steady hollow graphene nanospheres as an efficient electrocatalyst for the oxygen reduction reaction. *Adv Sci*. 2019;6(2):1801103.
60. Liu T, Li C, Yuan Q. Facile synthesis of PtCu alloy/graphene oxide hybrids as improved electrocatalysts for alkaline fuel cells. *ACS Omega*. 2018;3(8):8724-8732.
61. Guo Y, Tang J, Henzie J, et al. Assembly of hollow mesoporous nanoarchitectures composed of ultrafine Mo_2C nanoparticles on N-doped carbon nanosheets for efficient electrocatalytic reduction of oxygen. *Mater Horiz*. 2017;4(6):1171-1177.
62. Tan H, Li Y, Kim J, et al. Sub-50 nm iron-nitrogen-doped hollow carbon sphere-encapsulated iron carbide nanoparticles as efficient oxygen reduction catalysts. *Adv Sci*. 2018;5(7):1800120.
63. Tan H, Tang J, Henzie J, et al. Assembly of hollow carbon nanospheres on graphene nanosheets and creation of iron-nitrogen-doped porous carbon for oxygen reduction. *ACS Nano*. 2018;12(6):5674-5683.
64. Wang Y, Yang J, Sun S, et al. PtNi nanoparticles supported on electrochemically reduced porous graphene oxide for methanol oxidation reaction. *Chem Phys Lett*. 2019;730:575-581.
65. Ren F, Wang H, Zhai C, et al. Clean method for the synthesis of reduced graphene oxide-supported PtPd alloys with high electrocatalytic activity for ethanol oxidation in alkaline medium. *ACS Appl Mater Interfaces*. 2014;6(5):3607-3614.
66. Zhang K, Zhang LL, Zhao X, Wu J. Graphene/polyaniline nanofiber composites as supercapacitor electrodes. *Chem Mater*. 2010;22(4):1392-1401.
67. Ye Y-S, Cheng M-Y, Xie X-L, et al. Alkali doped polyvinyl alcohol/graphene electrolyte for direct methanol alkaline fuel cells. *J Power Sources*. 2013;239:424-432.
68. Lee DC, Yang HN, Park SH, Kim WJ. Nafion/graphene oxide composite membranes for low humidifying polymer electrolyte membrane fuel cell. *J Membr Sci*. 2014;452:20-28.
69. Jia W, Tang B, Wu P. Novel slightly reduced graphene oxide based proton exchange membrane with constructed long-range ionic nanochannels via self-assembling of nafion. *ACS Appl Mater Interfaces*. 2017;9(27):22620-22627.
70. Qiu X, Dong T, Ueda M, Zhang X, Wang L. Sulfonated reduced graphene oxide as a conductive layer in sulfonated poly(ether ether ketone) nanocomposite membranes. *J Membr Sci*. 2017;524:663-672.
71. Jiang ZJ, Jiang Z, Tian X, Luo L, Liu M. Sulfonated holey graphene oxide (SHGO) filled sulfonated poly(ether ether ketone) membrane: the role of holes in the SHGO in improving its performance as proton exchange membrane for direct methanol fuel cells. *ACS Appl Mater Interfaces*. 2017;9(23):20046-20056.
72. Liu L, Tong C, He Y, Zhao Y, Lü C. Enhanced properties of quaternized graphenes reinforced polysulfone based composite anion exchange membranes for alkaline fuel cell. *J Membr Sci*. 2015;487:99-108.
73. Tateishi H, Hatakeyama K, Ogata C, et al. Graphene oxide fuel cell. *J Electrochem Soc*. 2013;160(11):F1175-F1178.

74. Dikin DA, Stankovich S, Zimney EJ, et al. Preparation and characterization of graphene oxide paper. *Nature*. 2007;448(7152):457-460.
75. Gao W, Wu G, Janicke MT, et al. Ozonated graphene oxide film as a proton-exchange membrane. *Angew Chem Int Ed Engl*. 2014;53(14):3588-3593.
76. Holmes SM, Balakrishnan P, Kalangi VS, et al. 2D crystals significantly enhance the performance of a working fuel cell. *Adv Energy Mater*. 2017;7(5):1601216.
77. Yan XH, Wu R, Xu JB, Luo Z, Zhao TS. A monolayer graphene – Nafion sandwich membrane for direct methanol fuel cells. *J Power Sources*. 2016;311:188-194.
78. Vinayan BP, Nagar R, Rajalakshmi N, Ramaprabhu S. Novel platinum-cobalt alloy nanoparticles dispersed on nitrogen-doped graphene as a cathode electrocatalyst for PEMFC applications. *Adv Funct Mater*. 2012;22(16):3519-3526.
79. Liang Y, Li Y, Wang H, et al. Co_3O_4 nanocrystals on graphene as a synergistic catalyst for oxygen reduction reaction. *Nat Mater*. 2011;10(10):780-786.
80. Zhou Y, Yen CH, Hu YH, et al. Making ultrafine and highly-dispersive multimetallic nanoparticles in three-dimensional graphene with supercritical fluid as excellent electrocatalyst for oxygen reduction reaction. *J Mater Chem A*. 2016;4(47):18628-18638.
81. Li Y, Zhou Y, Zhu C, et al. Porous graphene doped with Fe/N/S and incorporating Fe_3O_4 nanoparticles for efficient oxygen reduction. *Catal Sci Technol*. 2018;8(20):5325-5333.
82. Zhang Q, Guan J. Single-atom catalysts for electrocatalytic applications. *Adv Funct Mater*. 2020;30(31):2000768.
83. Zhang C, Sha J, Fei H, et al. Single-atomic ruthenium catalytic sites on nitrogen-doped graphene for oxygen reduction reaction in acidic medium. *ACS Nano*. 2017;11(7):6930-6941.
84. Shu Y, Miyake K, Quílez-Bermejo J, et al. Rational design of single atomic Co in CoN_x moieties on graphene matrix as an ultra-highly efficient active site for oxygen reduction reaction. *ChemNanoMat*. 2020;6(2):218-222.
85. Mou X, Wang D, Liu X, Liu W, Cao L, Yao T. XAFS study on single-atomic-site Cu_1/N-graphene catalyst for oxygen reduction reaction. *Radiat Phys Chem*. 2020;175:108230.
86. Wen X, Bai L, Li M, Guan J. Atomically dispersed cobalt- and nitrogen-codoped graphene toward bifunctional catalysis of oxygen reduction and hydrogen evolution reactions. *ACS Sustain Chem Eng*. 2019;7(10):9249-9256.
87. Bai L, Duan Z, Wen X, Guan J. Bifunctional atomic iron-based catalyst for oxygen electrode reactions. *J Catal*. 2019;378:353-362.
88. Bai L, Hou C, Wen X, Guan J. Catalysis of oxygen reduction reaction on atomically dispersed copper- and nitrogen-codoped graphene. *ACS Appl Energy Mater*. 2019;2(7):4755-4762.
89. Bai L, Duan Z, Wen X, Si R, Guan J. Atomically dispersed manganese-based catalysts for efficient catalysis of oxygen reduction reaction. *Appl Catal B*. 2019;257:117930.
90. Wen X, Duan Z, Bai L, Guan J. Atomic scandium and nitrogen-codoped graphene for oxygen reduction reaction. *J Power Sources*. 2019;431:265-273.
91. Guan J, Wen X, Zhang Q, Duan Z. Atomic rhodium catalysts for hydrogen evolution and oxygen reduction reactions. *Carbon*. 2020;164:121-128.
92. Bai L, Duan Z, Wen X, Si R, Zhang Q, Guan J. Highly dispersed ruthenium-based multifunctional electrocatalyst. *ACS Catalysis*. 2019;9(11):9897-9904.
93. Chen S, Zhang N, Narváez Villarrubia CW, et al. Single Fe atoms anchored by short-range ordered nanographene boost oxygen reduction reaction in acidic media. *Nano Energy*. 2019;66:104164.
94. Yang L, Cheng D, Xu H, et al. Unveiling the high-activity origin of single-atom iron catalysts for oxygen reduction reaction. *Proc Natl Acad Sci*. 2018;115(26):6626-6631.
95. Zhang C, Liu J, Ye Y, Aslam Z, Brydson R, Liang C. Fe-N-doped mesoporous carbon with dual active sites loaded on reduced graphene oxides for efficient oxygen reduction catalysts. *ACS Appl Mater Interfaces*. 2018;10(3):2423-2429.
96. Asset T, Atanassov P. Iron-nitrogen-carbon catalysts for proton exchange membrane fuel cells. *Joule*. 2020;4(1):33-44.
97. Byon HR, Suntivich J, Shao-Horn Y. Graphene-based non-noble-metal catalysts for oxygen reduction reaction in acid. *Chem Mater*. 2011;23(15):3421-3428.
98. Chen X, Yu L, Wang S, Deng D, Bao X. Highly active and stable single iron site confined in graphene nanosheets for oxygen reduction reaction. *Nano Energy*. 2017;32:353-358.
99. Zitolo A, Goellner V, Armel V, et al. Identification of catalytic sites for oxygen reduction in iron- and nitrogen-doped graphene materials. *Nat Mater*. 2015;14(9):937-942.
100. Chung HT, Cullen DA, Higgins D, et al. Direct atomic-level insight into the active sites of a high-performance PGM-free ORR catalyst. *Science*. 2017;357(6350):479-484.
101. Xu H, Cheng D, Cao D, Zeng XC. A universal principle for a rational design of single-atom electrocatalysts. *Nat Catal*. 2018;1(5):339-348.
102. Xiao Y, Zhang W. High-throughput calculation investigations on the electrocatalytic activity of codoped single metal-nitrogen embedded in graphene for ORR mechanism. *Electrocatalysis*. 2020;11(4):393-404.
103. Mao X, Kour G, Yan C, Zhu Z, Du A. Single transition metal atom-doped graphene supported on a nickel substrate: enhanced oxygen reduction reactions modulated by electron coupling. *J Phys Chem C*. 2019;123(6):3703-3710.
104. Sun J, Lowe SE, Zhang L, et al. Ultrathin nitrogen-doped holey carbon@graphene bifunctional electrocatalyst for oxygen reduction and evolution reactions in alkaline and acidic media. *Angew Chem Int Ed Engl*. 2018;57(50):16511-16515.
105. Geng D, Chen Y, Chen Y, et al. High oxygen-reduction activity and durability of nitrogen-doped graphene. *Energy Environ Sci*. 2011;4(3):760.
106. Lai L, Potts JR, Zhan D, et al. Exploration of the active center structure of nitrogen-doped graphene-based catalysts for oxygen reduction reaction. *Energy Environ Sci*. 2012;5(7):7936-7942.
107. Wu J, Ma L, Yadav RM, et al. Nitrogen-doped graphene with pyridinic dominance as a highly active and stable electrocatalyst for oxygen reduction. *ACS Appl Mater Interfaces*. 2015;7(27):14763-14769.
108. Guo DH, Shibuya R, Akiba C, Saji S, Kondo T, Nakamura J. Active sites of nitrogen-doped carbon materials for oxygen reduction reaction clarified using model catalysts. *Science*. 2016;351(6271):361-365.
109. Yang Z, Yao Z, Li G, et al. Sulfur-doped graphene as an efficient metal-free cathode catalyst for oxygen reduction. *ACS Nano*. 2012;6(1):205-211.
110. Zhang L, Niu J, Li M, Xia Z. Catalytic mechanisms of sulfur-doped graphene as efficient oxygen reduction reaction catalysts for fuel cells. *J Phys Chem C*. 2014;118(7):3545-3553.

111. Sheng Z-H, Gao H-L, Bao W-J, Wang F-B, Xia X-H. Synthesis of boron doped graphene for oxygen reduction reaction in fuel cells. *J Mater Chem*. 2012;22(2):390-395.
112. Kong X, Chen Q, Sun Z. Enhanced oxygen reduction reactions in fuel cells on H-decorated and B-substituted graphene. *ChemPhysChem*. 2013;14(3):514-519.
113. Zhang C, Mahmood N, Yin H, Liu F, Hou Y. Synthesis of phosphorus-doped graphene and its multifunctional applications for oxygen reduction reaction and lithium ion batteries. *Adv Mater*. 2013;25(35):4932-4937.
114. Lin H, Chu L, Wang X, et al. Boron, nitrogen, and phosphorous ternary doped graphene aerogel with hierarchically porous structures as highly efficient electrocatalysts for oxygen reduction reaction. *New J Chem*. 2016;40(7):6022-6029.
115. Zhang J, Dai L. Nitrogen, phosphorus, and fluorine tri-doped graphene as a multifunctional catalyst for self-powered electrochemical water splitting. *Angew Chem Int Ed Engl*. 2016;55(42):13296-13300.
116. Yoo E, Okata T, Akita T, Kohyama M, Nakamura J, Honma I. Enhanced electrocatalytic activity of Pt subnanoclusters on graphene nanosheet surface. *Nano Lett*. 2009;9(6):2255-2259.
117. Zhang L-S, Liang X-Q, Song W-G, Wu Z-Y. Identification of the nitrogen species on N-doped graphene layers and Pt/NG composite catalyst for direct methanol fuel cell. *Phys Chem Chem Phys*. 2010;12(38):12055-12059.
118. Xiong B, Zhou Y, Zhao Y, et al. The use of nitrogen-doped graphene supporting Pt nanoparticles as a catalyst for methanol electrocatalytic oxidation. *Carbon*. 2013;52:181-192.
119. Singh RN, Awasthi R. Graphene support for enhanced electrocatalytic activity of Pd for alcohol oxidation. *Catal Sci Technol*. 2011;1(5):778.
120. Sun H, Ye Y, Liu J, et al. Pure Ni nanocrystallines anchored on rGO present ultrahigh electrocatalytic activity and stability in methanol oxidation. *Chem Commun*. 2018;54(13):1563-1566.
121. Li Y, Zhang L, Hu Z, Yu JC. Synthesis of 3D structured graphene as a high performance catalyst support for methanol electro-oxidation. *Nanoscale*. 2015;7(25):10896-10902.
122. Jang HD, Kim SK, Chang H, et al. Three-dimensional crumpled graphene-based platinum–gold alloy nanoparticle composites as superior electrocatalysts for direct methanol fuel cells. *Carbon*. 2015;93:869-877.
123. Qiu X, Yan X, Cen K, Sun D, Xu L, Tang Y. Achieving highly electrocatalytic performance by constructing holey reduced graphene oxide hollow nanospheres sandwiched by interior and exterior platinum nanoparticles. *ACS Appl Energy Mater*. 2018;1(5):2341-2349.
124. Gao Z, Li M, Wang J, et al. Pt nanocrystals grown on three-dimensional architectures made from graphene and MoS_2 nanosheets: highly efficient multifunctional electrocatalysts toward hydrogen evolution and methanol oxidation reactions. *Carbon*. 2018;139:369-377.
125. Yan M, Jiang Q, Zhang T, et al. Three-dimensional low-defect carbon nanotube/nitrogen-doped graphene hybrid aerogel-supported Pt nanoparticles as efficient electrocatalysts toward the methanol oxidation reaction. *J Mater Chem A*. 2018;6(37):18165-18172.
126. Yang C, Jiang Q, Li W, et al. Ultrafine Pt nanoparticle-decorated 3D hybrid architectures built from reduced graphene oxide and MXene nanosheets for methanol oxidation. *Chem Mater*. 2019;31(22):9277-9287.
127. Wang C, Wang H, Zhai C, et al. Three-dimensional $Au_{0.5}$/reduced graphene oxide/$Au_{0.5}$/reduced graphene oxide/carbon fiber electrode and its high catalytic performance toward ethanol electrooxidation in alkaline media. *J Mater Chem A*. 2015;3(8):4389-4398.
128. Huang W, Ma XY, Wang H, et al. Promoting effect of $Ni(OH)_2$ on palladium nanocrystals leads to greatly improved operation durability for electrocatalytic ethanol oxidation in alkaline solution. *Adv Mater*. 2017;29(37):1703057.
129. Liu J, Zheng Y, Hong Z, Cai K, Zhao F, Han H. Microbial synthesis of highly dispersed PdAu alloy for enhanced electrocatalysis. *Sci Adv*. 2016;2(9):e1600858.
130. Shen Y, Gong B, Xiao K, Wang L. In situ assembly of ultrathin PtRh nanowires to graphene nanosheets as highly efficient electrocatalysts for the oxidation of ethanol. *ACS Appl Mater Interfaces*. 2017;9(4):3535-3543.
131. Yang H, Li S, Feng F, et al. Palladium nanoparticles with surface enrichment of palladium oxide species immobilized on the aniline-functionalized graphene as an advanced electrocatalyst of ethanol oxidation. *ACS Sustain Chem Eng*. 2019;7(17):14621-14628.
132. Chowdhury SR, Maiyalagan T, Bhattachraya SK, Gayen A. Influence of phosphorus on the electrocatalytic activity of palladium nickel nanoalloy supported on N-doped reduced graphene oxide for ethanol oxidation reaction. *Electrochim Acta*. 2020;342:136028.
133. Luo L, Fu C, Yang F, et al. Composition-graded Cu–Pd nanospheres with Ir-doped surfaces on N-doped porous graphene for highly efficient ethanol electro-oxidation in alkaline media. *ACS Catalysis*. 2019;10(2):1171-1184.
134. Yao C, Zhang Q, Su Y, et al. Palladium nanoparticles encapsulated into hollow N-doped graphene microspheres as electrocatalyst for ethanol oxidation reaction. *ACS Appl Nano Mater*. 2019;2(4):1898-1908.
135. Fan X, Yuan W, Zhang DH, Li CM. Heteropolyacid-mediated self-assembly of heteropolyacid-modified pristine graphene supported Pd nanoflowers for superior catalytic performance toward formic acid oxidation. *ACS Appl Energy Mater*. 2018;1(2):411-420.
136. Shen W, Ge L, Sun Y, et al. Rhodium nanoparticles/F-doped graphene composites as multifunctional electrocatalyst superior to Pt/C for hydrogen evolution and formic acid oxidation reaction. *ACS Appl Mater Interfaces*. 2018;10(39):33153-33161.
137. Feng JJ, Chen SS, Chen XL, Zhang XF, Wang AJ. One-pot fabrication of reduced graphene oxide supported dendritic core-shell gold@gold-palladium nanoflowers for glycerol oxidation. *J Colloid Interface Sci*. 2018;509:73-81.
138. Qi J, Benipal N, Wang H, et al. Metal-catalyst-free carbohydrazide fuel cells with three-dimensional graphene anodes. *Chemsuschem*. 2015;8(7):1147-1150.
139. Yong YC, Yu YY, Zhang X, Song H. Highly active bidirectional electron transfer by a self-assembled electroactive reduced-graphene-oxide-hybridized biofilm. *Angew Chem Int Ed Engl*. 2014;53(17):4480-4483.
140. Luo J, Jang HD, Sun T, et al. Compression and aggregation-resistant particles of crumpled soft sheets. *ACS Nano*. 2011;5(11):8943-8949.
141. Ren H, Tian H, Gardner CL, Ren TL, Chae J. A miniaturized microbial fuel cell with three-dimensional graphene macroporous scaffold anode demonstrating a record power density of over 10,000 W m^{-3}. *Nanoscale*. 2016;8(6):3539-3547.

142. Yang Y, Liu T, Zhu X, et al. Boosting power density of microbial fuel cells with 3D nitrogen-doped graphene aerogel electrode. *Adv Sci*. 2016;3(8):1600097.
143. Chen JY, Xie P, Zhang ZP. Reduced graphene oxide/polyacrylamide composite hydrogel scaffold as biocompatible anode for microbial fuel cell. *Chem Eng J*. 2019;361:615-624.
144. Song R-B, Zhou S, Guo D, et al. Core/satellite structured Fe_3O_4/Au nanocomposites incorporated with three-dimensional macroporous graphene foam as a high-performance anode for microbial fuel cells. *ACS Sustain Chem Eng*. 2019;8(2):1311-1318.
145. Li J, Yu Y, Chen D, et al. Hydrophilic graphene aerogel anodes enhance the performance of microbial electrochemical systems. *Bioresour Technol*. 2020;304:122907.
146. Jiang G, Goledzinowski M, Comeau FJE, et al. Free-standing functionalized graphene oxide solid electrolytes in electrochemical gas sensors. *Adv Funct Mater*. 2016;26(11):1729-1736.
147. Ye Y-S, Tseng C-Y, Shen W-C, et al. A new graphene-modified protic ionic liquid-based composite membrane for solid polymer electrolytes. *J Mater Chem*. 2011;21(28):10448.
148. Aragaw BA, Su W-N, Rick J, Hwang B-J. Highly efficient synthesis of reduced graphene oxide–Nafion nanocomposites with strong coupling for enhanced proton and electron conduction. *RSC Adv*. 2013;3(45):23212.
149. Chien H-C, Tsai L-D, Huang C-P, Kang C-Y, Lin J-N, Chang F-C. Sulfonated graphene oxide/Nafion composite membranes for high-performance direct methanol fuel cells. *Int J Hydrogen Energy*. 2013;38(31):13792-13801.
150. Ren YJ, Anisur MR, Qiu W, He JJ, Al-Saadi S, Singh Raman RK. Degradation of graphene coated copper in simulated proton exchange membrane fuel cell environment: electrochemical impedance spectroscopy study. *J Power Sources*. 2017;362:366-372.
151. Raghupathy Y, Kamboj A, Rekha MY, Narasimha Rao NP, Srivastava C. Copper-graphene oxide composite coatings for corrosion protection of mild steel in 3.5% NaCl. *Thin Solid Films*. 2017;636:107-115.
152. Sim Y, Kwak J, Kim S-Y, et al. Formation of 3D graphene–Ni foam heterostructures with enhanced performance and durability for bipolar plates in a polymer electrolyte membrane fuel cell. *J Mater Chem A*. 2018;6(4):1504-1512.
153. Jiang X, Drzal LT. Exploring the potential of exfoliated graphene nanoplatelets as the conductive filler in polymeric nanocomposites for bipolar plates. *J Power Sources*. 2012;218:297-306.
154. Plengudomkit R, Okhawilai M, Rimdusit S. Highly filled graphene-benzoxazine composites as bipolar plates in fuel cell applications. *Polym Compos*. 2016;37(6):1715-1727.
155. Jiang L, Syed JA, Lu H, Meng X. In-situ electrodeposition of conductive polypyrrole-graphene oxide composite coating for corrosion protection of 304SS bipolar plates. *J Alloys Compd*. 2019;770:35-47.
156. Mišković-Stanković V, Jevremović I, Jung I, Rhee K. Electrochemical study of corrosion behavior of graphene coatings on copper and aluminum in a chloride solution. *Carbon*. 2014;75:335-344.
157. Pu N-W, Shi G-N, Liu Y-M, et al. Graphene grown on stainless steel as a high-performance and ecofriendly anti-corrosion coating for polymer electrolyte membrane fuel cell bipolar plates. *J Power Sources*. 2015;282:248-256.
158. Kong W, Kum H, Bae SH, et al. Path towards graphene commercialization from lab to market. *Nat Nanotechnol*. 2019;14(10):927-938.
159. Kurapova OY, Glukharev AG, Glumov OV, Kurapov MY, Boltynjuk EV, Konakov VG. Structure and electrical properties of YSZ-rGO composites and YSZ ceramics, obtained from composite powder. *Electrochim Acta*. 2019;320:134573.

How to cite this article: Su H, Hu YH. Recent advances in graphene-based materials for fuel cell applications. *Energy Sci Eng*. 2020;00:1–26. https://doi.org/10.1002/ese3.833